Chemistry
A European
Journal

Chemistry Europe
European Chemical Societies Publishing

Accepted Article

Title: Tweaking the Optoelectronic Properties of S-Doped Polycyclic Aromatic Hydrocarbons by Chemical Oxidation

Authors: Oliwia Matuszewska, Tommaso Battisti, Ruben R. Ferreira, Nicolas Biot, Nicola Demitri, Cécile Mézière, Magali Allain, Marc Sallé, Samuel Mañas-Valero, Eugenio Coronado, Elisa Fresta, Rubén D. Costa, and Davide Bonifazi

To be cited as: *Chem. Eur. J.* **2022**, e202203115

Link to VoR: https://doi.org/10.1002/chem.202203115

WILEY-VCH

Tweaking the Optoelectronic Properties of S-Doped Polycyclic Aromatic Hydrocarbons by Chemical Oxidation

Oliwia Matuszewska[+],[a] Tommaso Battisti[+],[a] Ruben R. Ferreira,[b] Nicolas Biot,[a] Nicola Demitri,[c] Cécile Mézière,[d] Magali Allain,[d] Marc Sallé,[d] Samuel Mañas-Valero,[e] Eugenio Coronado,[e] Elisa Fresta,[f] Rubén D. Costa*,[f] and Davide Bonifazi*[a,b]

[a] School of Chemistry, Cardiff University, Main Building, Park Place, Cardiff CF10 3AT, United Kingdom.

[b] Institute of Organic Chemistry, University of Vienna, 1090 Vienna, Austria. E-mail: davide.bonifazi@univie.ac.at

[c] Elettra – Sincrotrone Trieste, S.S. 14 Km 163.5 in Area Science Park, 34149 Basovizza, Trieste, Italy.

[d] MOLTECH-Anjou - UMR CNRS 6200, UNIV Angers, SFR Matrix, 2 Boulevard Lavoisier, 49045 Angers Cedex, France.

[e] Instituto de Ciencia Molecular, Universitat de València, Catedrático José Beltrán 2, 46980 Paterna, Spain.

[f] Chair of Biogenic Functional Materials, Technical University Munich, Schulgasse 22, Straubing D-94315, Germany. E-mail: ruben.costa@tum.de

[+] These authors contributed equally to this manuscript

Supporting information for this article is given via a link at the end of the document.

Abstract: *Peri*-thiaxanthenothiaxanthene, an S-doped analog of *peri*-xanthenoxanthene, is used as a polycyclic aromatic hydrocarbon (PAH) scaffold to tune the molecular semiconductor properties by editing the oxidation state of the S-atoms. Chemical oxidation of *peri*-thiaxanthenothiaxanthene with H_2O_2 led to the relevant sulfoxide and sulfone congeners, whereas electrooxidation gave access to sulfonium-type derivatives forming crystalline mixed valence (MV) complexes. These complexes depicted peculiar molecular and solid-state arrangements with face-to-face π-π stacking organization. Photophysical studies showed a widening of the optical bandgap upon progressive oxidation of the S-atoms, with the bis-sulfone derivative displaying the largest value (E_{00} = 2.99 eV). While *peri*-thiaxanthenothiaxanthene showed reversible oxidation properties, the sulfoxide and sulfone derivatives mainly showed reductive events, corroborating their *n*-type properties. Electric measurements of single crystals of the MV complexes exhibited a semiconducting behavior with a remarkably high conductivity at room temperature (10^{-1}-10^{-2} S cm^{-1} and 10^{-2}-10^{-3} S cm^{-1} for the O and S derivatives, respectively), one of the highest reported so far. Finally, the electroluminescence properties of the complexes were tested in light-emitting electrochemical cells (LECs), obtaining the first S-doped mid-emitting PAH-based LECs.

10.1002/chem.202203115

Introduction

Replacing the carbon atoms with isostructural atoms at given positions is a functionalization strategy to tailor the chemical, optoelectronic and self-assembly properties of molecular and macromolecular polycyclic aromatic hydrocarbons (PAHs).[1–3] While B,[4–7] N[8–10] and P[11–15] heteroatoms can replace both the core and peripheral C(sp2) atoms, the use of chalcogen atoms is fundamentally restricted to the doping of the peripheries. Noticeable examples include O-,[16] S-,[17–19] Se-[20–22] and Te-doped[23,24] structures. In recent years, our group became interested in the development of novel O-doped PAHs.[25–27] In particular, we became interested in the O-containing congener of anthanthrene, *peri*-xanthenoxanthene (PXX),[28–31] and developed synthetic strategies to prepare molecular ribbons[32,33] and mono/diimide[34,35] derivatives. It was observed that the insertion of O-atoms induces a rising of the highest occupied molecular orbital (HOMO) energy level, *p*-type behaviour.[29,31,36,37]

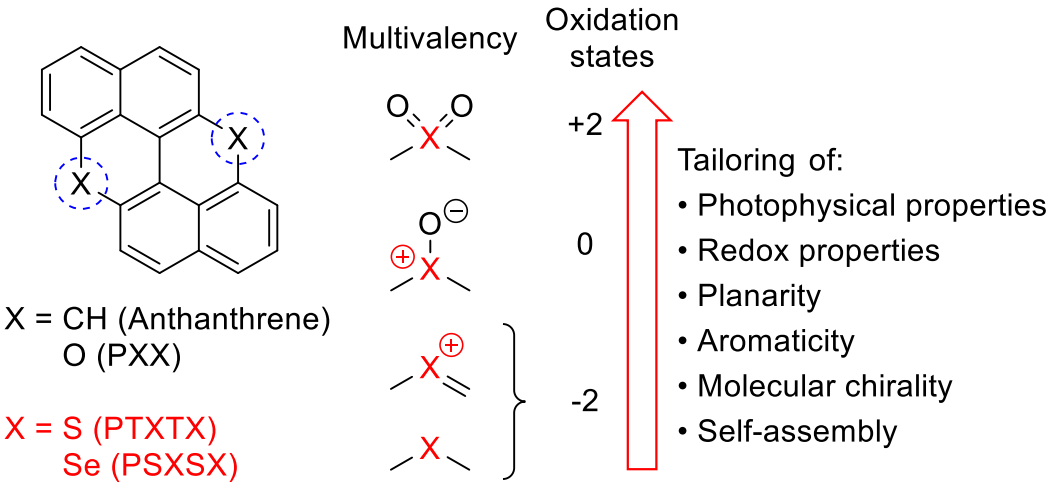

Fig. 1. S and Se-doped anthanthrenes and their multivalent species.

The oxidation of the pyrano-derived aromatics readily gives access to stable pyrylium cations, featuring significantly red-

shifted UV-vis absorption spectra when compared to their neutral forms.[38,39] However, the narrow multivalency space of the oxygen atom limits the structural and optoelectronic variabilities that one can access through chemical editing of the heteroatom valency (*i.e.*, through oxidation). In contrast, the other chalcogen atoms, S, Se and Te atoms, feature a large multivalency space (from II to VI).[40] Thus, we conjectured that peri-thiaxanthenothiaxanthene (**4^{H}**), the S-doped congener of **PXX** in which the O-atoms are replaced by S-atoms,[41,42] could be an ideal structural motif to engineer PAHs, whose optoelectronic properties are tailored by tweaking the chalcogen-atoms valency through oxidation (Fig. 1). In particular, it is expected that mono- and di-oxidation of the S-atoms could be reflected in the widening of the molecular HOMO-LUMO gap, rising of the ionization potential and inducing a perturbation of the conformational properties that rule the solid-state organization. Indulging this line of thought, herein we report on the preparation, solid-state organization and optoelectronic properties of the sulfoxide, sulfone and sulfonium derivatives of *peri*-thiaxanthenothiaxanthene (**PTXTX**). Building on the same synthetic strategy, the synthesis of the Se-congener peri-selenoxanthenoselenoxanthene (**PSXSX**) is also reported. The electrical and electroluminescent behaviours of the most relevant and chemically inert derivatives have been analysed and the first mid-energy emitting performing PHA-based light-emitting electrochemical cells (LECs) have been realised.

Results and discussion.

Synthesis and structural characterization of the sulfoxide and sulfone derivatives. Dibromo-1,1'-binaphthalene **1** was reacted with *n*-BuLi in the presence of TMEDA followed by the addition of $(MeS)_2$,[43] providing intermediate dimethylthiobinaphthalene **2^{H}** in 79% yield (Scheme 1). Subsequent bromination with Br_2 afforded

compound **2^{Br}** in 90% yield that, under Kumada cross-coupling conditions with OctylMgBr, afforded derivative **2^{Oct}** (70%).

a) *peri*-thiaxanthenothiaxanthene scaffolding

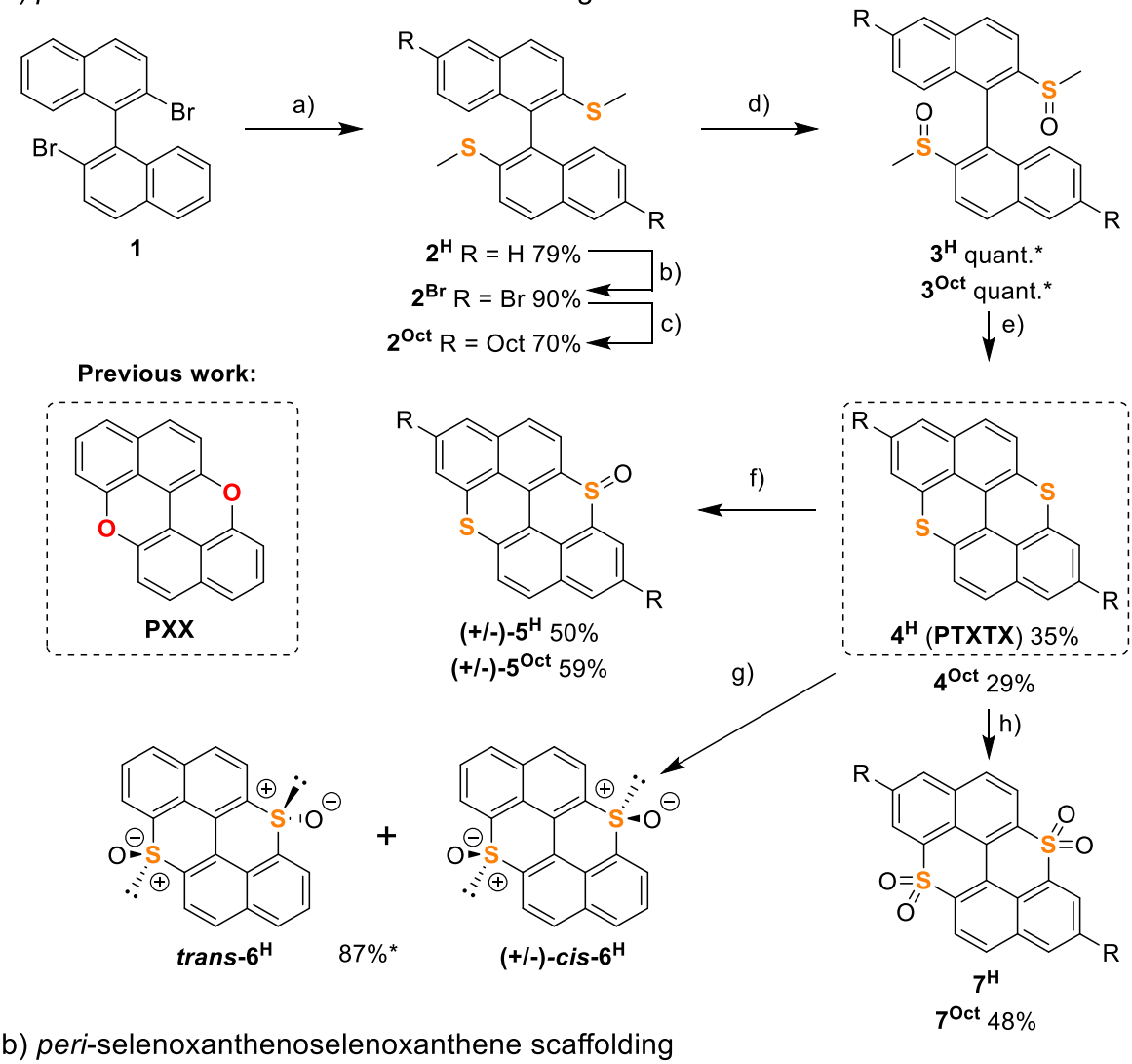

b) *peri*-selenoxanthenoselenoxanthene scaffolding

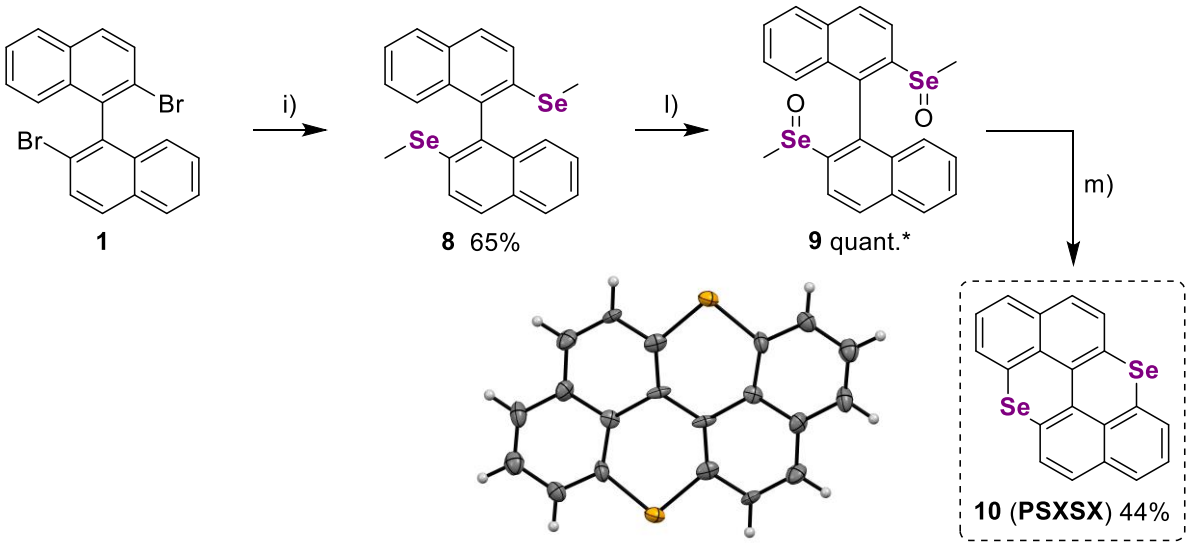

Scheme 1. a) 1. *n*-BuLi, TMEDA, THF, -94°C to 0°C, under N_2, 1 h; 2. Me_2S_2, -94°C to rt, under N_2, overnight; b) Br_2, CH_2Cl_2, under N_2, 0°C to rt, overnight; c) OctMgBr, THF, [Pd(dppf)Cl_2], under N_2, reflux 2,5 h, rt, overnight; d) H_2O_2, CH_3COOH, $CHCl_3$, rt, 5 h; e) 1. TfOH, under N_2, rt, 24 h; 2. Pyridine/H_2O, 100 °C, 1 h; f) H_2O_2, CH_3COOH, $CHCl_3$, rt, 6 h; g) H_2O_2, CH_3COOH, $CHCl_3$, rt, 24 h; h) H_2O_2, CH_3COOH, reflux, overnight; i) 1. *n*-BuLi, TMEDA, THF, -78°C, 1h, under N_2; 2. Me_2Se_2, under N_2, from -78°C to rt, overnight; l) H_2O_2, AcOH, $CHCl_3$, rt; m) 1. TfOH, 80°C, under N_2, overnight; 2. Pyridine, 100°C, under N_2, overnight. *yield of the diastereoisomeric mixture. X-ray structure of molecule **10**; space group: $P2_1/c$; atom colors: orange Se, grey C.

Oxidation of molecules $\mathbf{2^H}$ and $\mathbf{2^{Oct}}$ with H_2O_2 in $CH_3COOH/CHCl_3$ quantitatively afforded desired disulfoxide derivatives $\mathbf{3^H}$ and $\mathbf{3^{Oct}}$ as diastereoisomeric mixtures.[18] Friedel-Craft cyclization in TfOH, followed by demethylation reaction in a pyridine/H_2O mixture, [44,45] gave derivatives $\mathbf{4^H}$ and $\mathbf{4^{Oct}}$ as orange solids in 35% and 29% yield, respectively. Subsequent oxidation of $\mathbf{4^H}$ and $\mathbf{4^{Oct}}$ in $CH_3COOH/CHCl_3$ with six and eight eq. of H_2O_2 afforded sulfoxides (±)-$\mathbf{5^H}$ and (±)-$\mathbf{5^{Oct}}$ in 50% and 59% yield, respectively. When 20 eq. of H_2O_2 were used, disulfoxide $\mathbf{6^H}$ was instead obtained as a mixture of *trans* (***t*-6H**) and *cis* ((±)-$\boldsymbol{c}$-$\mathbf{6^H}$) isomers in 87% yield. While the *cis* isomer rapidly decomposes on SiO_2, $\boldsymbol{t}$-$\mathbf{6^H}$ could be isolated as a pure product. Traces of the sulfone-sulfoxide conjugate were also isolated as confirmed by X-ray diffraction analysis (see the X-ray structure shown in Fig. S94, of molecule $\mathbf{11^H}$). Despite a few attempts, we could not prepare the sulfone-sulfoxide conjugate selectively and isolate it with sufficient purity under our experimental conditions. When a large excess of H_2O_2 in CH_3COOH is used under reflux conditions for 16 h, molecules $\mathbf{4^H}$ and $\mathbf{4^{Oct}}$ oxidize to the disulfones ($\mathbf{7^H}$ and $\mathbf{7^{Oct}}$). While the alkylated derivative $\mathbf{7^{Oct}}$ could be isolated (48% yield) and characterized, unsubstituted compound $\mathbf{7^H}$ is insoluble in common organic solvents. Prompted by these results, we also explored the possibility to extend this synthetic strategy to

the preparation of the Se-congener, **PSXSX**, and of its oxidized derivatives. Thus, reaction of **1** with *n*-BuLi with TMEDA followed by the addition of $(MeSe)_2$ gave dimethylselenobinaphthalene **8** in 65% yield (Scheme 1). Oxidation with H_2O_2 in $CH_3COOH/CHCl_3$ quantitatively afforded selenoxide **9** as a mixture of diastereoisomers. Friedel-Craft cyclization with neat TfOH followed by demethylation gave targeted Se-doped anthanthrene **10** (**PSXSX**) as poorly soluble solid in 44%. Unlikely **PTXTX**, attempts to oxidize **PSXSX** to either its selenoxide or selenium dioxide derivatives proved to be unsuccessful and gave decomposition products. All molecules were characterized by NMR techniques, HR-MS spectrometry and, when possible, single-crystal X-ray diffraction. Due to its low solubility, derivative $\mathbf{7^H}$ was characterized only by mass and X-ray analyses.

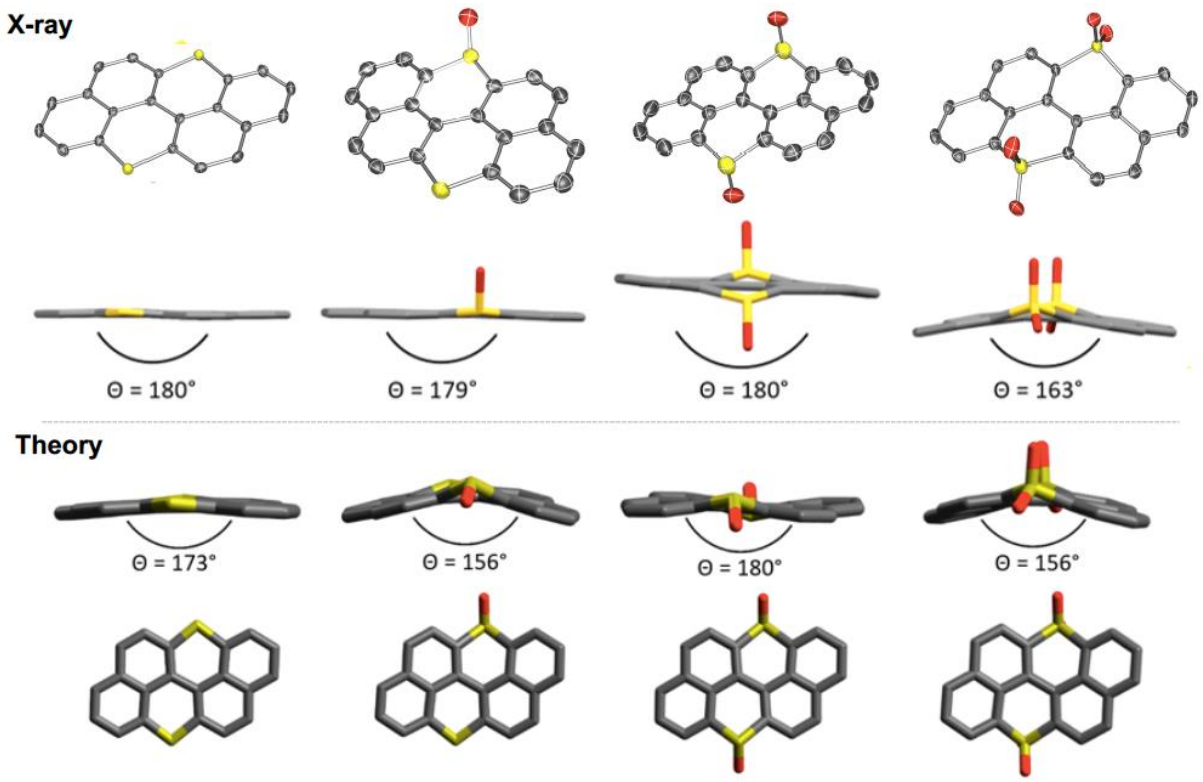

Fig. 2. Crystal (*top*) and calculated at the B3LYP/cc-pVTZ level of theory (bottom) structures for PAHs $\mathbf{4^H}$, $\mathbf{5^H}$, ***t*-6^H** and $\mathbf{7^H}$. Space groups for crystals are: $P2_1/c$, $P2_12_12_1$, $P2_1/c$, and P-1, respectively. The **Θ** value is the angle that is formed between the planes comprising the two naphthalenyl rings. Atom colors: red O, yellow S, grey C. Theoretical calculations in vacuum reported consistent conformations to those observed experimentally for molecules $\mathbf{4^H}$, $\mathbf{5^H}$, $\mathbf{7^H}$, and ***t*-6^H**.

Crystallization of compounds **4^{H}**, **4^{oct}**, **5^{H}**, ***t*-6^{H}**, **7^{H}**, **7^{Oct}**, and **10** for X-ray diffraction analysis were successful (Fig. 2), while all attempts to obtain crystals of ***c*-6^{H}** failed. Single crystals of **4^{H}** were prepared by slow diffusion of EtOH vapors into CH_2Cl_2, giving rise to two polymorphic crystals: yellow plates (Fig. S85A, polymorph A) and red needles (Fig. S86A, polymorph B). The polymorphs show similar bonds lengths and angles within the experimental errors (d_{C-S} = 1.741(2) Å; C-S-C angle = 103.9(1)° for the plates and d_{C-S} = 1.739(5) - 1.740(5) Å; C-S-C angle = 104.0(2) - 104.1(2)° for the plates *vs* d_{C-O} = 1.389(1) – 1.391(1) Å and C-O-C angle = 118.80(8)° for **PXX**).[46] A lamellar-type organization driven by the interdigitation of the octyl chains was observed instead for the X-ray structure of molecule **4^{oct}** (Fig. S87). Crystals suitable for X-ray for Se-congener **10** were obtained by hot crystallization from a 1:1 toluene and hexane mixture (Scheme 1). Similarly to molecule **4^{H}**, the naphthyl rings are co-planar. The C-Se-C angle is 100.1(6)°, which is significantly lower than the C-S-C and C-O-C angles measured for **PTXTX** (103.9(1)°) and **PXX** (118.80(8)°). The length of C-Se bonds in **10** is 1.87(1) – 1.88(1) Å, which is longer than the corresponding C-S and C-O bonds in **PTXTX** (1.741(2) Å) and **PXX** (1.389(1) – 1.391(1) Å). The molecules arrange in π-π stacks (3.526 Å) organized in a slip-type fashion, similarly to the yellow-plate polymorph of **PTXTX**. Each stack interacts intercolumnary through Se···Se contacts ($d_{Se\cdots Se}$ = 3.658(2) Å).

Crystals of **5^{H}** were obtained by hot recrystallisation from CH_3CN. The X-ray structure confirmed the presence of sulfoxide moiety (Fig. 2). Notably, the C-S bond lengths of the thioether functions (d_{C-S} = 1.735(6) – 1.739(6) Å) are consistent with that observed for molecule **4^{H}**, whereas those of the sulfoxide moiety are 1.772(6) Å and 1.760(6) Å. Single crystals of ***t*-6^{H}** and **7^{Oct}** were grown by hot crystallization from DMSO. The X-ray analysis of ***t*-6^{H}** confirmed the *trans* disposition of the sulfoxide groups, whereas **7^{H}** showed the full oxidation of both thioether functions

10.1002/chem.202203115

to sulfones (Fig. 2). Notably, ***t*-6^{H}** displays a *saddle*-type distortion, with the two O-atoms situated in *pseudo-equatorial* positions. On the other hand, disulfone **7^{H}** adopts a slightly bent V-type conformation where two of the O-atoms are placed in *pseudo-axial* and two in *pseudo-equatorial* positions (Fig. 2). In this structure, the C-S bond lengths are 1.745(2) – 1.748(2) Å and 1.749(3) – 1.751(2) Å and are very similar to those observed in **5^{H}** (d_{C-S} = 1.735(6) – 1.739(6) Å). Notably, in all the oxidized derivatives, a network of weak H-bonding interactions is established between the O-atoms and the aromatic C-H (Fig. S88, S90 and S91), which is thought to be responsible for their low solubility. Crystals of derivative **7^{Oct}** were grown from slow diffusion of hexane into toluene. Notably, plate- and rod-like crystals were obtained belonging to the C2/c and $P2_1/c$ space groups, respectively (Fig. 4 and Fig. S92). When looking at the X-ray structures of **7^{Oct}** in the $P2_1/c$ crystals, one can notice the disulfone framework adopting an *anti*-type conformation (***anti*-7^{Oct}**), in which the two *pseudo-axial* and *pseudo-equatorial* O-atoms are *anti* (Fig. 3). On the other hand, in the C2/c polymorph, the *pseudo-axial* and *pseudo-equatorial* O-atoms are in a *syn*-type conformation, ***syn*-7^{Oct}** (Fig. 3).

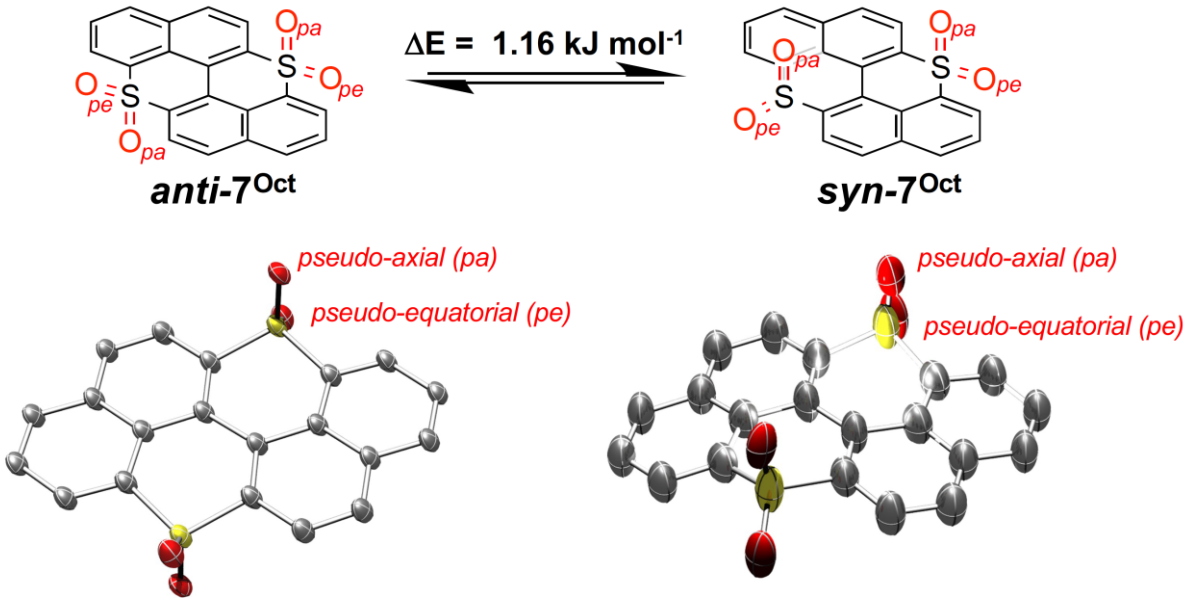

10.1002/chem.202203115

Fig. 3. Above: ***anti*-7^{Oct} *syn*-7^{Oct}** conformers (ΔE estimated by DFT calculations from the optimized structures in vacuum at the B3LYP/cc-pVTZ level of theory). Below: X-ray structures of **7^{Oct}** in polymorphs *P*2$_1$/*c* and *C*2/*c* as obtained by slow diffusion of hexane vapors into a toluene solution containing **7^{Oct}** (the octyl chains were not included in the calculations and have been omitted for clarity from this figure)). Atom colors: red O, yellow S, grey C.

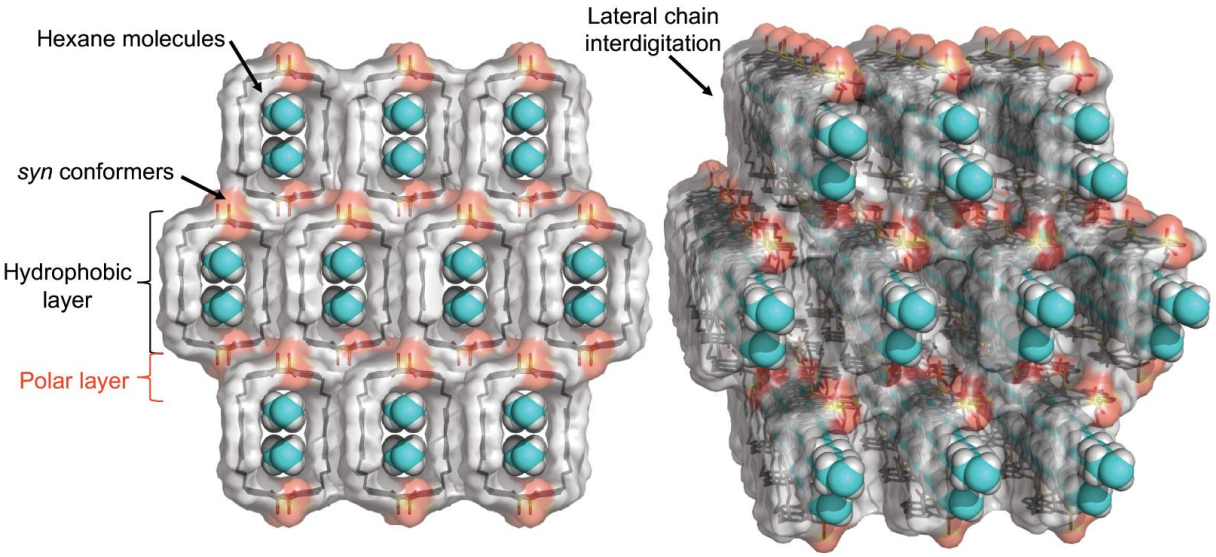

Fig. 4. Crystal structure of the organic hydrophobic clathrate made of ***syn*-7^{Oct}** encapsulating hexane molecules (cyan-coloured spheres) perfectly aligned with the pore channels. Space group: C2/c. Atom colors: red O, yellow S, grey C, green C atoms of the hexane molecules.

The interdigitation of the octyl chains of ***syn*-7^{Oct}** in the C2/c crystals allows for the entrapment of hexane solvent molecules forming clathrates (Fig. 4). Heating of the C2/c crystals induces the evaporation of the hexane molecules, leading to a collapse of the clathrate architecture with a consequent formation of P2$_1$/c crystals (Fig. S92). In these crystals, an in-plane interdigitation of the aliphatic chains is observed, with a consequent formation of a lamellar-type organization.

Photophysical and electrochemical characterization. The photophysical properties of **4^{H}**, **5^{H}**, ***t*-6^{H}**, **7^{Oct}** and **10** were investigated in CH_2Cl_2 and solid state (Table 1, Fig. 7). The absorption and emission spectra of molecule **4^{H}** are consistent with those of **PXX.**[26,34,46] The lowest-energy $\pi \rightarrow \pi^*$ transition absorption band of the former is bathochromically shifted (λ_{max} = 500 nm) compared to that of **PXX** (λ_{max} = 443 nm). In addition,

10.1002/chem.202203115

the presence of the heavier S atoms lessens the oscillator strength of the $S_0 \rightarrow S_1$ transition, broadening and reducing the intensity of the absorption band ($\epsilon_{max} \approx 7000$ $M^{-1}cm^{-1}$ and 17000 $M^{-1}cm^{-1}$ for **4^H** and **PXX**, respectively).[42,47] Compared to molecule **4^H**, the oxidations of S-atoms cause a progressive blue shift of the electronic transition energies. The lowest-energy bands of the absorption spectra of oxidized derivatives **5^H**, ***t*-6^H**, and **7^{Oct}** are centered at λ_{max} = 458 nm, 414 nm and 399 nm, respectively (Fig. 5). Emission profiles for molecules **4^H**, **5^H**, ***t*-6^H**, and **7^{Oct}** (CH_2Cl_2 at rt) mirror the absorption bands with pronounced vibronic substructures (Fig. 7). In addition, narrow Stokes' shifts (λ_{em} = 410, 410, 430, and 220 nm, respectively), moderated photoluminescence quantum yields (Φ_{em}) (Φ_{em} = 2%, 22%, 4%, and 35%, respectively) and lifetimes in the nanosecond range (τ = 5.2, 11.2, 0.6, and 0.7 ns, respectively) are observed.

10.1002/chem.202203115

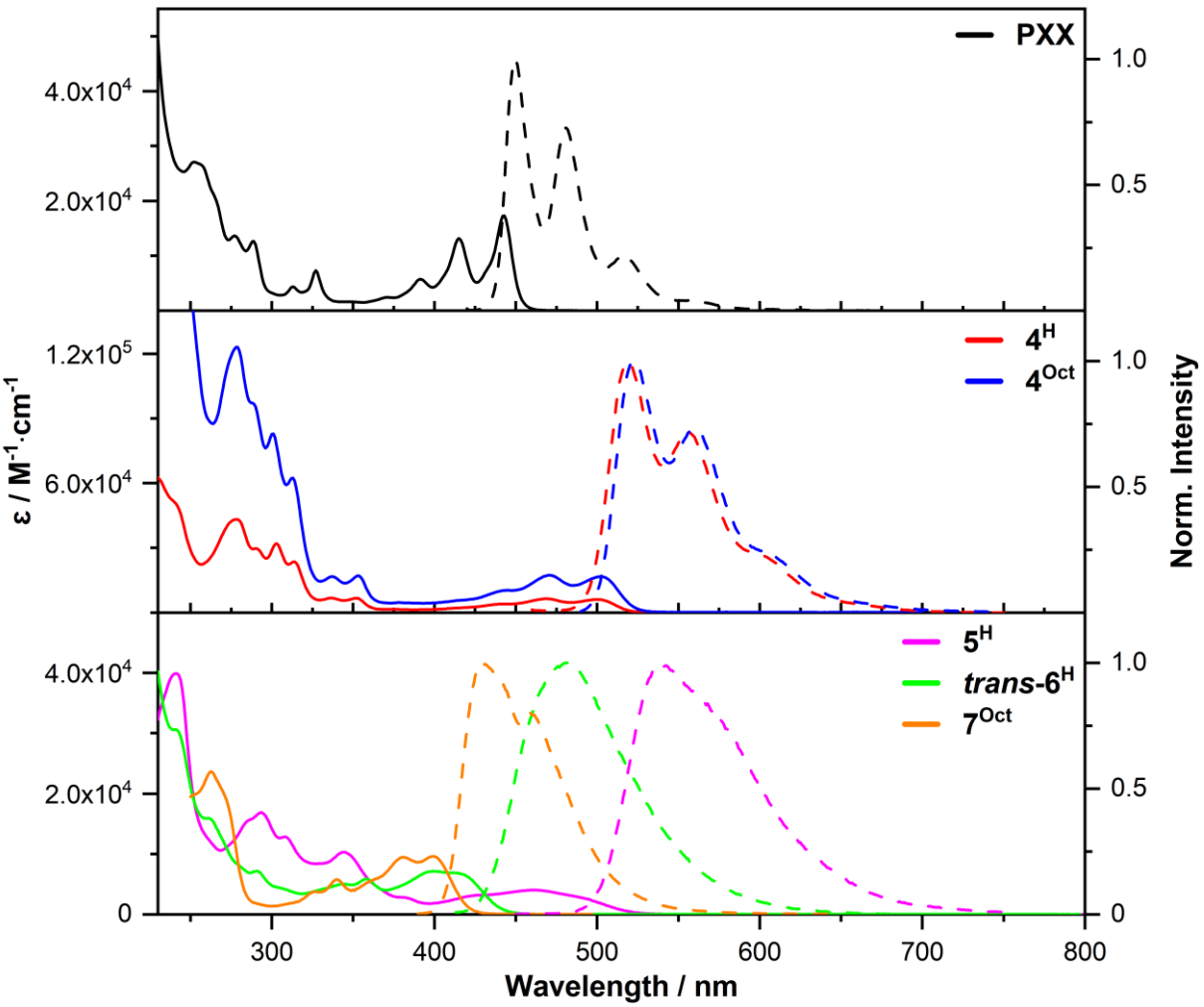

Fig. 5. Absorption (—) and fluorescence (---) spectra for **PXX** (black, λ_{exc} = 410 nm), **4^{H}** (red, λ_{exc} = 450 nm), **4^{Oct}** (blue, λ_{exc} = 470 nm), **7^{Oct}** (orange, λ_{exc} = 365 nm), ***t*-6^{H}** (green, λ_{exc} = 350 nm), and **5^{H}** (magenta, λ_{exc} = 345 nm) in aerated CH_2Cl_2 at rt.

The lower Φ_{em} value of **4^{H}** compared to that of **PXX** is ascribable to an efficient non-radiative deactivation via triplet population. This hypothesis was confirmed by $^1O_2$-sensitisation measurements, showing $^1O_2$ quantum yields ($\Phi_{rel}(^1O_2)$) of 0.26 and 0.64 for **PXX** and **4^{H}**, respectively (Fig. S22, Table S2). The triplet state population was furtherly verified experimentally by the detection of a phosphorescence peak for molecule **4^{H}** centered at λ = 700–820 nm (τ = 210 μs) at 77 K, induced by external heavy atom effect in the presence of CH_3I (Fig. S20).[48]

Table 1. Absorption and emission maxima, fluorescence lifetimes, and Φ_{em} recorded for molecules **4^{H}**, **5^{H}**, ***t*-6^{H}**, and **7^{Oct}** in aerated CH_2Cl_2 at rt.

	Absorption	Emission			Energy Band Gap	
Molecule	λ, nm (ε, M^{-1} cm^{-1})	λ_{max} (nm)	τ (ns)[a]	Φ_{em}	E_{00} (eV)[d]	E_g^T (eV)[e]
PXX	443 (17284)[34]	450[34]	5.0[34]	0.62[34][b]	2.78	3.30
4^{Oct}	502 (16728) 470 (17308)	523	6.5	0.48	2.44	2.35[g]
4^{H}	500 (6017) 469 (6367)	518	5.2	<0.02[b]	2.45(1.72)[f]	3.05
5^{H}	497 (2300) 461 (4017) 421 (2300)	539	11.2	0.22[b]	2.42	3.20
***t*-6^{H}**	420 (6323) 396 (7030)	483	0.6	0.04[b]	2.82	3.37
7^{Oct}	400(9603) 382 (9437)	430	0.7	0.35[c]	2.99	2.89[g]

[a]λ_{exc} = 450 or 340 nm. [b]Standard: coumarin 153 in EtOH (ϕ = 0.53).[49] [c]9,10-Diphenylanthracene in CHX (Φ= 0.97±0.03).[50] [d]Energy calculated at the lowest energy intersection (λ_{int}) between normalized absorption and emission spectra, E_{00} = 1240.5/λ_{int}. [e]Calculated bandgap at the B3LYP/cc-pVTZ level of a gas phased optimized geometry unless otherwise specified. [f]Energy gap between S_0 and T_1.[g]See figure S27.

As far as Se-derivative **10** is concerned, we noticed that small impurities of other emissive species were always present in solution, likely deriving from oxidation, preventing us from performing a comprehensive photophysical characterization (Fig. S21).

Cyclic voltammetry (CV) measurements were performed to investigate the molecules' redox properties (Table 2, Fig. S12-S19). Molecule **4^{H}** possesses a lower oxidation potential ($E_{1/2}^{ox_1}$ = 0.21 V) than **PXX** ($E_{1/2}^{ox_1}$ = 0.31 V), whereas oxidized derivatives **5^{H}**, ***t*-6^{H}** showed irreversible oxidative events. On the other hand, reversible reduction peaks were observed for **5^{H}**, ***t*-6^{H}**, and **7^{Oct}** ($E_{1/2}^{red_1}$= -1.90 V, -1.60 V and -1.34 V, respectively). A second reduction wave was also observed for derivatives ***t*-6^{H}** and **7^{Oct}** at $E_{1/2}^{red_2}$ = -1.96 V (irreversible) and -1.82 V (reversible), respectively. As expected, S-doping enhances the reduction

10.1002/chem.202203115

behavior compared to **PXX**. Orbital energy calculations performed on the optimized geometries in vacuum showed a lowering of the HOMO-LUMO energy bandgap upon substitution of the O with S atoms, along with its widening upon progressive oxidation (Fig. S26), confirming both the data obtained from the electrochemical and photophysical studies.

10.1002/chem.202203115

Table 2. Plot of $E_{1/2}^{ox_1}$ and $E_{1/2}^{red_1}$ vs the total number of oxygen atoms attached to S. CV data of **PXX**, **4^{H}**, **4^{Oct}**, **5^{H}**, ***t*-6^{H}**, **7^{Oct}**, **10** in CH_2Cl_2 at rt (scan rate: 0.05 V s^{-1}, $TBAPF_6$ as electrolyte (0.1 M), and Ferrocene as internal reference). Values between brackets represent the peak-to-peak separation of the reversible redox events. *Irreversible peaks.

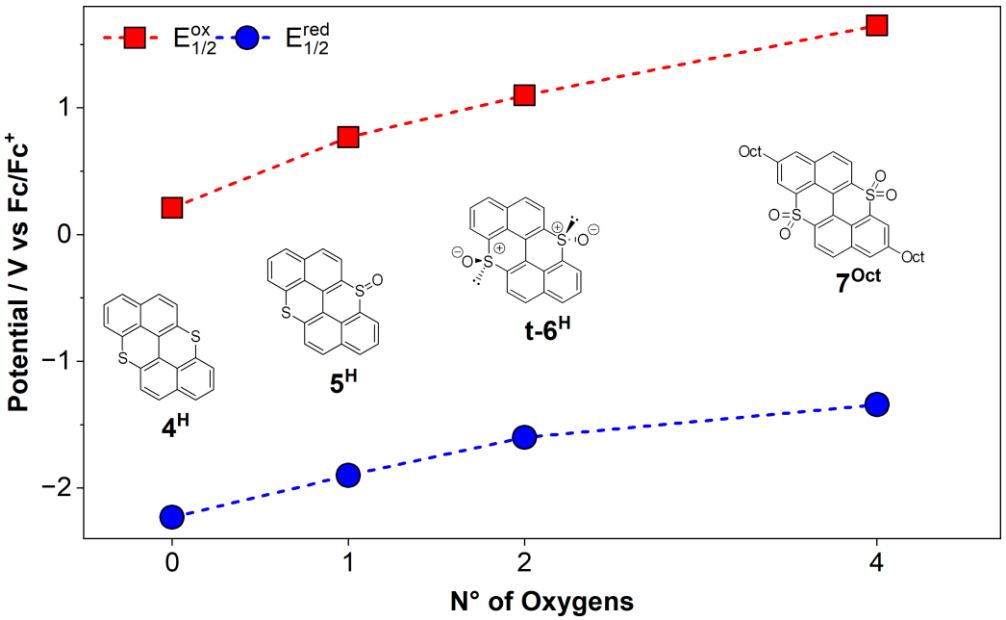

	Oxidations		Reductions	
Molecule	$E_{1/2}^{ox_1}$	$E_{1/2}^{ox_2}$	$E_{1/2}^{red_1}$	$E_{1/2}^{red_2}$
PXX	0.31(87)	-	-	-
4^{H}	0.21(97)	-	-	-
4^{Oct}	0.13(66)	0.74(74)	-	-
5^{H}	0.77*	1.23*	-1.90(100)	-
***t*-6^{H}**	1.10*	1.30*	-1.6(90)	-1.96*
7^{Oct}	-	-	-1.34(115)	-1.82(145)
10	0.16 (73)	0.69 (60)	-	-

Synthesis and structural characterization of sulfonium-type derivatives. Next, we performed electrooxidation experiments[38] to grow crystals of sulfonium-type cations of **4^{H}** and oxonium-type references of **PXX** (SI, Section 4). Attempts to provide crystals of oxidized species of **PSXSX** and **7^{Oct}** failed. Orthorhombic shiny black crystals containing salts of mixed-valence (MV) complexes for **PXX** were obtained in a solution of THF with 20% EtOH over a period of ten days (Fig. 5). On the

10.1002/chem.202203115

other hand, monoclinic black needles containing MV complexes of **4^{H}** were prepared in three days (Fig. 6). While **PXX** electro-crystallizes in an asymmetric unit containing two crystallographically-independent molecules and one ClO_4^- (WARNING: precautions need to be taken when dealing with perchlorates as they are potentially explosive), (**PXX**)$_2$(ClO_4)$_1$, the S-doped congener depicts three independent molecules and two ClO_4^- anions, (**4^{H}**)$_3$(ClO_4)$_2$.

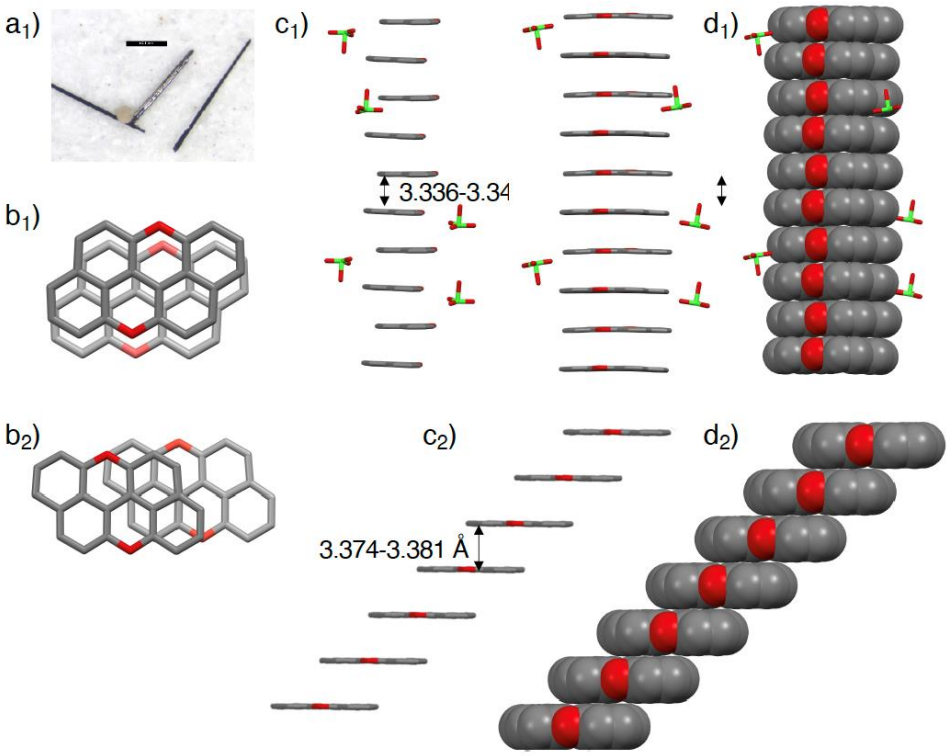

Fig. 6. X-ray structures and solid-state organization for MV complexes (**PXX**)$_2$(ClO_4)$_1$ (a1, b1, c1, d1) and reference neutral **PXX** (b2, c2, d2). a) Morphology of the crystals, b) X-ray structure of the relevant isolated O-doped molecules in their π-π stacking mode. c-d) Solid-state columnar π-π stacks. Atom colors: red O, grey C, green Cl.

Looking at organization at the solid state of (**PXX**)$_2$(ClO_4)$_1$ (Fig. 5b$_1$-d$_1$), one can evidence the presence of a columnar arrangement (Fig. 5b$_1$), with an average interplanar spacing of 3.33(7) Å (shortest distance between ring centroids of 3.367(12) Å with a lateral slippage of 0.83 Å). The ClO_4^- counterions are evenly intercalated in between the stacks (Fig. 5c$_1$). Similarly, in the crystal of (**4^{H}**)$_3$(ClO_4)$_2$ (Fig. 6b$_1$-d$_1$), the molecule solely

segregates in pillars of π-π stacks ($d_{π-π}$ = from 3.35 to 3.37 Å, Fig. 7c1), with ClO_4^- anions intercalating between different stacks. In contrast, neutral molecule **4H** arranges exclusively from typical herringbone organization in the neutral state (Fig. 6b2-d2), with the π-π stacks featuring different off-set depending on the polymorph. While in the red needles (polymorph B) the molecules are face-to-face off-set like in graphite-like arrangement (2.80 Å, 3.41 and 3.51 Å, Fig. S86), in the yellow crystals (polymorph A) π-π stacks organize in a slip-type fashion (1.79 Å, 3.45 Å, Fig. S85).

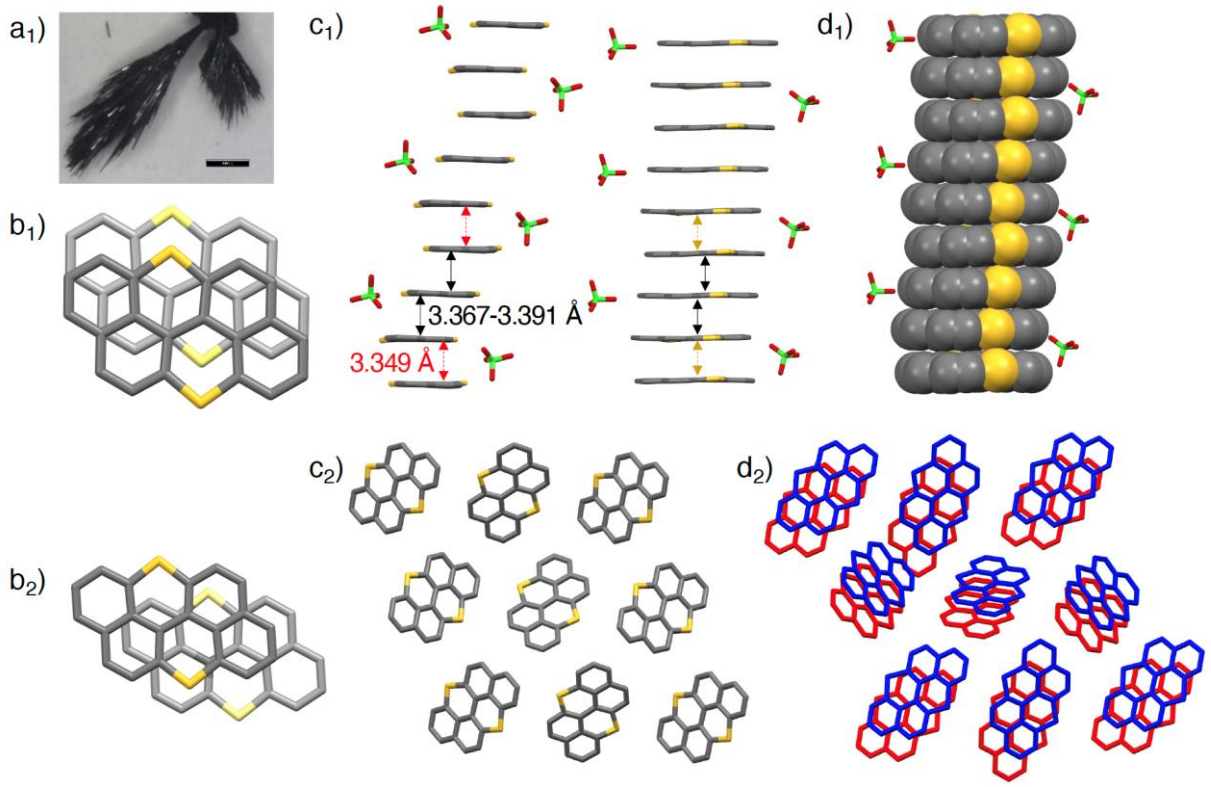

Fig. 7. X-ray structures and solid state organization for MV complexes $(\mathbf{4^H})_3(ClO_4)_2$ (a1,b1,c1,d1) *P*2$_1$/*c* and reference neutral **4H** (b2, c2, d2) *P*2$_1$/*c*. a) Morphology of the crystals; b) X-ray structure of the relevant isolated **4H** molecule in a stacking mode, c-d) solid-state columnar π-π stacks. For the MV complexes, two stacking modes between two **4H** molecules were observed. Atom colors: red O, grey C, green Cl, yellow S.

Electrical characterization of the mixed-valence complexes. Electric investigations of single crystals of both MV complexes $(\mathbf{PXX})_2(ClO_4)_1$ and $(\mathbf{4^H})_3(ClO_4)_2$ revealed a semiconducting behavior with ohmic I-V curves (a few crystals were measured for each

material, see SI Section 5).[51] The conductivities (σ) at rt are in the order of 10^{-2}–10^{-3} S cm^{-1} for $(\mathbf{4^H})_3(ClO_4)_2$ and 10^{-1}–10^{-2} S cm^{-1} for $(\mathbf{PXX})_2(ClO_4)_1$. The temperature dependence of the conductivity in the range of 150 K and 300 K (Fig. 8) can be modelled by considering single activation energy in the Arrhenius plots, with average E_a = 175 meV and 70 meV for $(\mathbf{4^H})_3(ClO_4)_2$ and $(\mathbf{PXX})_2(ClO_4)_1$, respectively (See SI). Except for TCNQ-TTF co-crystals, and a few examples of MOFs and radicals, generally organic semiconducting materials are insulators or weakly conductive (σ <10^{-6} S cm^{-1} at 300 K). If compared to previous organic mixed-valence complexes obtained by us previously with O-doped PAHs,[38] which featured σ_{ohmic} = 8.8×10^{-5} and 3.7×10^{-3} S cm^{-1}; $\sigma_{non-ohmic}$ = 2.4×10^{-4} and 5.1×10^{-3} S cm^{-1}, both $(\mathbf{PXX})_2(ClO_4)_1$ and $(\mathbf{4^H})_3(ClO_4)_2$ MV crystals display one of the best conductivity values for an organic semiconductor to date.

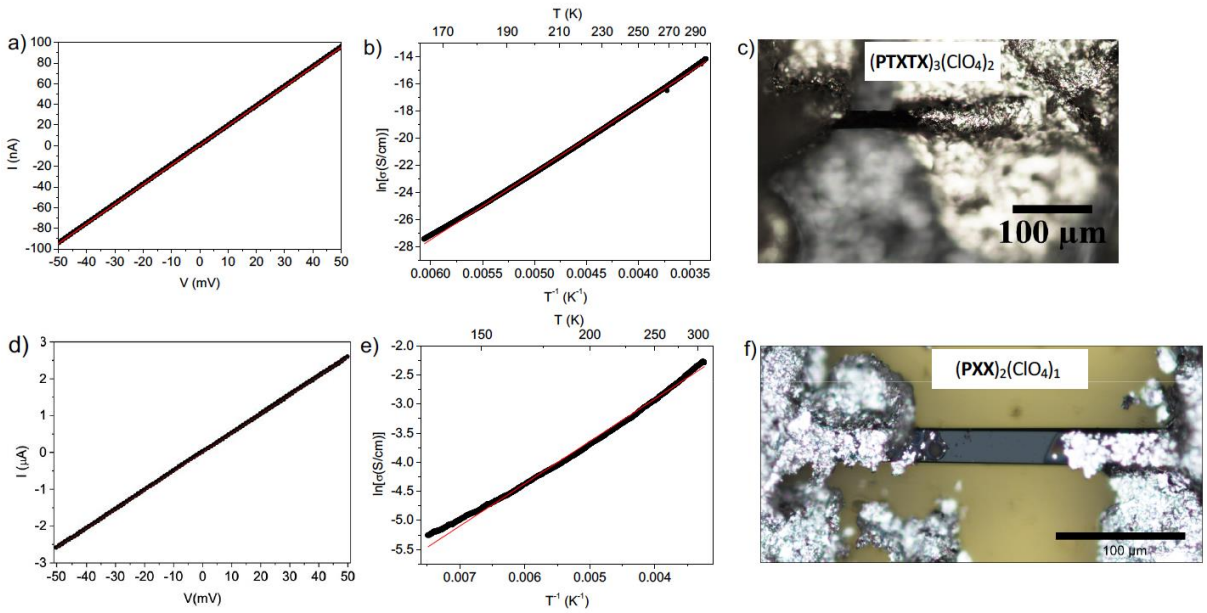

Fig. 8. Device and electrical response of crystals of $(\mathbf{4^H})_3(ClO_4)_2$ (a-c) and $(\mathbf{PXX})_2(ClO_4)_1$ (d-f). a) and d) I-V curves (•••) at 300K with the ohmic linear fit (–); for $(\mathbf{4^H})_3(ClO_4)_2$: ohmic fit ($R^2$ = 0.99998), slope 1.8982 ± 0.0005×10^{-6} Ω^{-1}, *y*-intercept 2.6 ± 0.2×10^{-10} A; for $(\mathbf{PXX})_2(ClO_4)_1$: ohmic fit ($R^2$ = 0.99995), slope 5.169 ± 0.003×10^{-5} Ω^{-1}, *y*-intercept 4.3 ± 0.8×10^{-9} A. b) and e) Arrhenius plot of the conductivity *vs*. temperature (•••) together with the linear fit (–). For $(\mathbf{4^H})_3(ClO_4)_2$ and $(\mathbf{PXX})_2(ClO_4)_1$: E_a = 185.29 ± 0.02 meV (R^2 = 0.99931) and E_a = 62.83 ± 0.07 meV (R^2 = 0.99466), respectively; Top views of the single crystal devices c) and f). The conductivity and activation energy values are referred to the specific devices displayed in c) and f) pictures (more data are reported in the SI).

Electroluminescence behavior in LEC. Light-emitting electrochemical cells (LECs) are thin-film lighting devices based on a blend of an electroluminescent material and an ionic electrolyte sandwiched between two air-stable electrodes.[52–54] They are characterized by a low-cost and easy-to-upscale fabrication process with solution-based techniques (i.e., spray coating, gravure printing), high tolerance towards the type of electrodes and the active layer thickness, and high versatility with respect to the type of emitters and ionic electrolyte.[53,54] In this context, PAHs emitters, such as twisted nanographene,[55] BN-doped coronene,[56,57] pentacene,[58] pyrene[59–62] derivatives, have explored realizing highly performing blue- or deep-red emitting LECs. However, mid-energy emitting PAH-based LECs have not been realized yet. Considering the yellowish green emission of the PTXTX-type derivatives and their *p*-type semiconducting properties, we conjectured that the unoxidized derivatives of PTXTX (*i.e.*, **4^{H}** and **4^{oct}**) could be implemented as emissive layers in LECs. Thin films (thickness of *ca.* 60 nm) were fabricated onto quartz and Indium Tin Oxide (ITO) substrates using a mixture of the emitters and the ionic matrix, namely trimethylolpropane ethoxylate (TMPE) and potassium triflate (KOTf) in a 1:0.10:0.02 ratio (emitter:TMPE:KOTf). While **4^{H}**, **5^{H}**, ***t*-6^{H}** and **10** did not show enough solubility in common solvents to process thin-films *via* spin-coating, those with **4^{oct}** along with reference **PXX** and **7^{oct}** were fabricated. Atomic force microscopy (AFM) assays of **4^{oct}** and **PXX** films showed a homogeneous morphology with root mean square (RMS) roughness of 3 nm (Fig. S8).

Table 3. Thin-film photophysical properties of **7^{oct}**, **4^{oct}**, and **PXX** films.

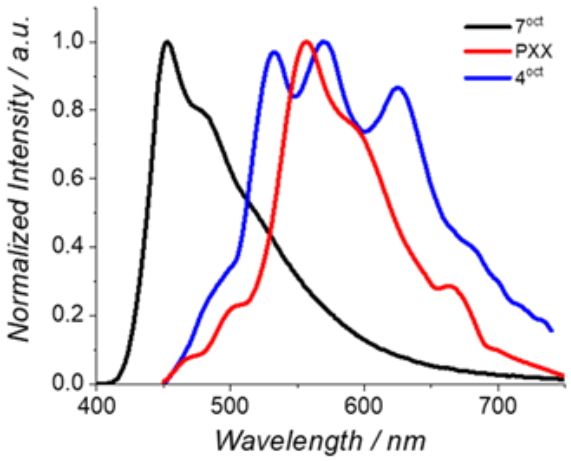

	$\lambda_{max}{}^{a}$ (nm)	$\lambda_{max}{}^{b}$ (nm)	$\Phi_{em}{}^{film a}$	$\Phi_{em}{}^{film b}$	τ^{a} (nm)	τ^{b} (nm)
7^{oct}	453 481	455 481	0.22	0.25	2.9	3.1
4^{oct}	530 571 625	533 567 627	0.07	0.10	1.0	0.9
PXX	465 504 551	450 512 546	0.48	0.46	6.6	5.2

[a]Only emitter (λ_{exc}=377 nm); [b]with polyelectrolyte matrix (λ_{exc}=377 nm).

In contrast, films containing reference **7^{oct}** displayed the presence of aggregates regardless of the efforts to optimize the solvent mixtures, concentrations, ionic matrix composition, and deposition technique. All films showed a similar photoluminescence spectrum to that observed in solution, with a less-structured and slightly red-shifted emission bands (**7^{oct}**: λ_{max} = 453 nm, with a shoulder at 481 nm, **4^{oct}**: λ_{max} = 571 nm with shoulders at 530 and 625 nm, **PXX**: λ_{max} = 551 nm with further peaks at 465 and 504 nm, Table 3). This goes along with photoluminescence quantum yields $\Phi_{em}{}^{film}$ of 0.25 (**7^{oct}**), 0.10 (**4^{oct}**) and 0.46 (**PXX**) and average excited state lifetimes <τ> in the ns-regime (Table 3). Noteworthy, the thin-film emission profile and properties (<τ> and $\Phi_{em}{}^{film}$) of the emitters are not affected by the presence of the ionic matrix (Fig. S9, Table 3). Notably, the emission band shape holds upon increasing the temperature from 77 K to 373 K (Fig. S10), suggesting a stable device color

at high and low applied currents.[56,57] Despite the film morphology, the electroluminescent behavior of **7^{oct}**, **4^{oct}** and **PXX** was studied in LECs built as ITO/PEDOT:PSS (90 nm)/**PXX**, **7^{oct}** or **4^{oct}**:TMPE:KOTf 1:0.10:0.02 (60 nm)/Al(90 nm). They were first tested using repetitive L-I-V (luminance-current intensity-voltage) scans at a speed of 300 mV s^{-1} (Fig. 9). As expected from the electrochemical assays, **7^{oct}**-based devices did not show any electroluminescence responses (Fig. S11), as the exciton formation is strongly hindered by the lack of oxidation processes. This contrasts with previous works on phenothiazine-based LECs, in which the oxidized derivative shows a similar blue-shifted emission band, but a suitable redox behavior for LECs.[63] **4^{oct}**-based and **PXX**-based devices showed a similar charge injection behavior with a significant electroluminescence response, reaching maximum luminance values of 10 cd m^{-2} and 75 cd m^{-2}, respectively, which are in line with the $\Phi_{em}{}^{film}$ values of the films (Table 3). The electroluminescence responses correspond to a broad emission band centered at 494 nm and 537 nm for **PXX** and **4^{oct}** (Fig. 9) respectively, featuring an overall chromaticity similar to that of the photoluminescence outputs of the films and solutions (i.e., green and green-yellow responses with x/y CIE of 0.31/0.52 and 0.36/0.52, respectively). Finally, the electroluminescence spectra do not change upon increasing the applied bias and under repetitive LIV scans (Fig. 9), suggesting good stability upon charge injection.

10.1002/chem.202203115

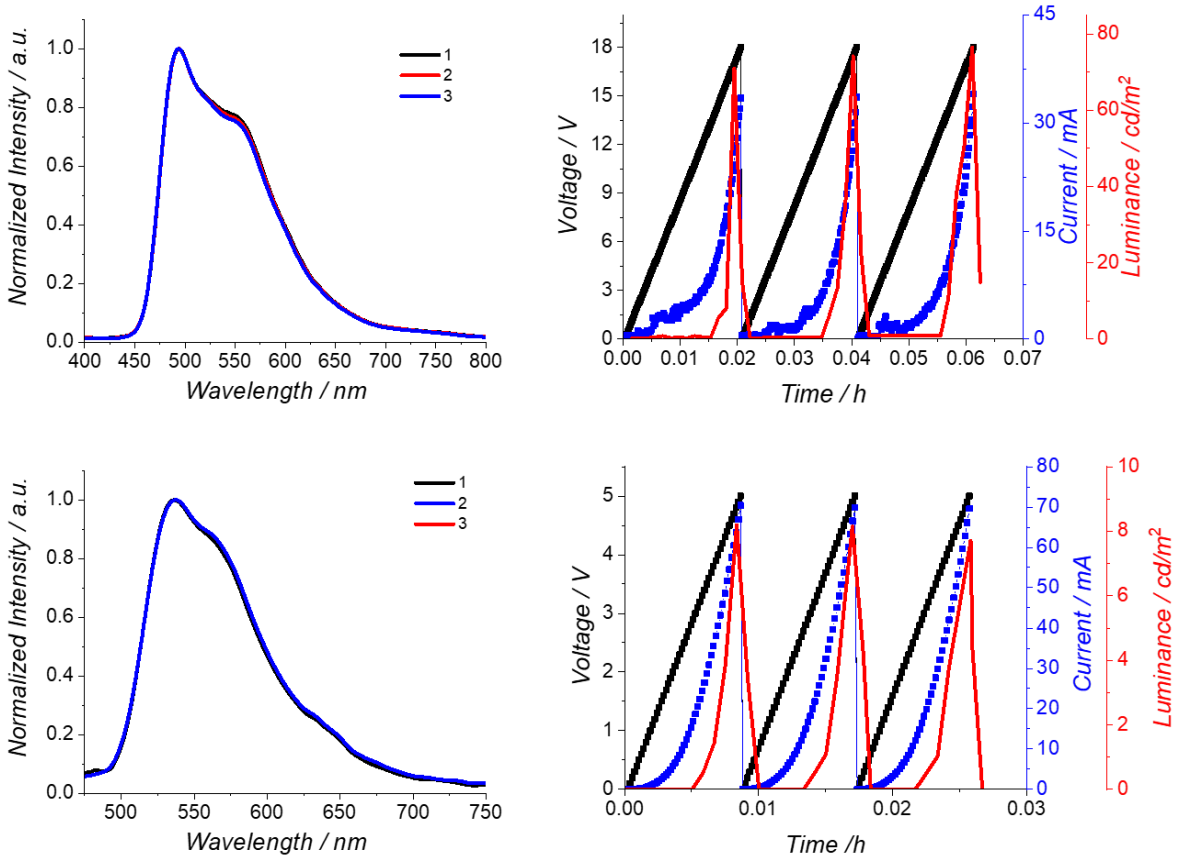

Fig. 9. Electroluminescence spectra at 5 V upon repetitive L-I-V scans (see legend) and voltage, current and luminance in repetitive L-I-V scans (right) of **PXX**- (top) and **4**^{oct}-based (bottom) LECs.

The devices were measured at different pulsed currents (1,000 Hz and 50% duty cycle) of 10 and 20 mA (Table 4 and Fig. 10). Both devices show the typical LEC behavior with respect to a high initial applied voltage that rapidly drops due to the formation of electrical double layers at the electrode surfaces leading to an enhanced charge injection process. At this stage, the applied voltage remains in a plateau regime, indicating that the layers are free of pin-hole or black-spot formations (electrochemical damage) related to irreversible device degradation.[52] Finally, the luminance enhances upon formation of the electric double layers (EDLs), reaching the maximum values followed by a quick exponential decay.

10.1002/chem.202203115

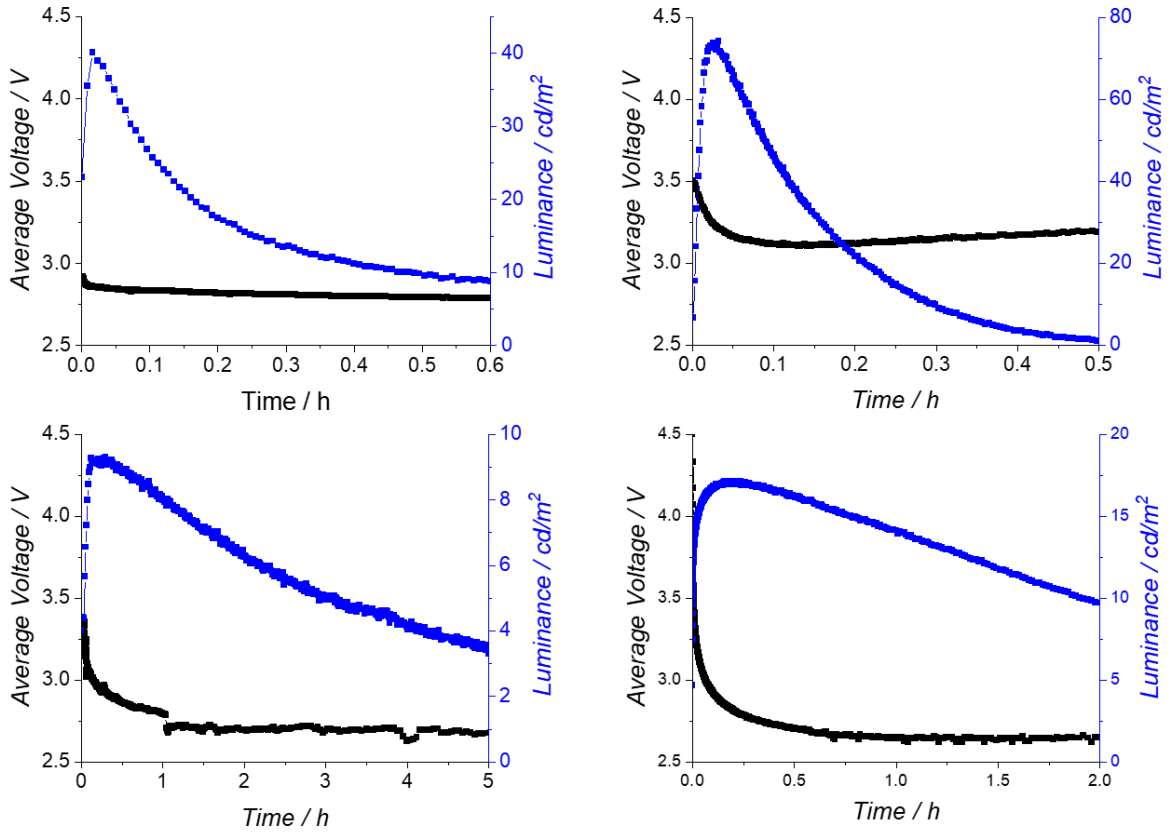

Fig. 10. Average voltage and luminance over time of **PXX**- (top) and **4^{oct}**- (bottom) based LECs driven at pulsed 10 mA (left) and 20 mA (right).

Overall, the devices with **PXX** show good performances with a maximum luminance of *ca.* 40 and 75 cd m^{-2} associated with an average efficacy of 0.1 cd/A at 10 and 20 mA, respectively.

Table 4. **PXX**- and **4^{oct}**-based LECs measured at different pulsed currents.

Device	PC[a] (mA)	Luminance$_{max}$[b] (cd m^{-2})	Average Voltage (V)	$t_{1/2}$[c] (h)	E_{tot}[d] (mJ)	Eff[e] (cd/A)
PXX	10 mA	40.1	2.7	0.3	31.0	0.08
PXX	20 mA	74.2	3.2	0.2	36.5	0.07
4^{oct}	10 mA	9.4	2.6	3.2	82.6	0.02
4^{oct}	20 mA	17.3	2.7	2.2	79.4	0.01

[a]PC: pulsed current. [b]Maximum luminance. [c]Time to reach 50% of the initial luminance. [d]Total emitted energy. [e]Power efficiency

As expected from the reduced $\Phi_{em}{}^{film}$ **4^{oct}** films, these devices showed lower luminance values of *ca.* 10 and 17 cd m^{-2} along with lower efficiencies (Table 4). Finally, the device stability of a few hours is similar for both emitters. While these devices

are the first examples of mid-emitting S-doped PAH-based LECs, their performance is also comparable to that of the sate-of-art of green-emitting LECs based on small molecules (e.g., efficiency of 0.1-2 cd/A, and stability, when measured of only a few hours), [56,60,64-67] attributed to unbalanced charge injection. Considering that both **4^{oct}** and **PXX** compounds possess a strong *n*-type character, unbalanced charge injection and growing of the doped region must be present. This prompted us to conclude that neutral emitting zone in the *p*-i-*n* junction is established close to the metal cathode, leading to a prominent exciton quenching and a poor light out-coupling.[68]

Conclusions

This paper reports a comprehensive study on *peri*-thiaxanthenothiaxanthenes as novel semiconducting PAHs. The chemical oxidation of **4^{H}** with H_2O_2 gave access to the relevant mono- and di- sulfoxides and sulfone derivatives, whereas electro-oxidation yielded sulfonium-type derivatives as mixed-valence (MV) architectures. Se-doped analogue **PSXSX** was also prepared following the same synthetic approach, but could not be selectively oxidized to provide the selenoxide or selenium dioxide derivatives. The relevant oxidized species were characterized by X-ray crystallography, which revealed peculiar conformational properties in the solid state. Photophysical studies showed that a widening of the optical bandgap could be achieved upon progressive oxidation of the S-atoms, with the bis-sulfone derivative depicting the most significant value. While non-oxidized **PTXTX** displayed *p*-type properties, the oxidized products expressed an *n*-type behavior as indicated by reversible reductive processes. Electric measurements of single crystals of MV salts of the oxonium- and sulfonium-type derivatives, exhibited a semiconducting behavior with very high conductivity at room temperature (10^{-1}-10^{-2} S cm^{-1} and 10^{-2}-10^{-3} S cm^{-1}, respectively). Finally, integrating the PTXTX-based

derivatives as emissive materials into LECs led to the first mid-emitting devices with performances similar to the state-of-art small molecule-based LECs.[56,60,65,66,69,70]

Experimental Section

Chemicals were purchased from Sigma Aldrich, Acros Organics, Alfa Aesar, Apollo Scientific, TCI and Fluorochem and were used as received. Solvents were purchased from Sigma Aldrich, while deuterated solvents from Eurisotop. Dry THF and CH_2Cl_2 were prepared as needed by drying HPLC grade solvents using a Braun MB SPS-800 solvent purification system. Nuclear magnetic resonance spectra were recorded on a Bruker Fourier 300 MHz spectrometer equipped with a dual (^{13}C, ^{1}H) probe, a Bruker AVANCE III HD 400MHz NMR spectrometer equipped with a Broadband multinuclear (BBFO) SmartProbe™ or a Bruker AVANCE III HD 500MHz Spectrometer equipped with Broadband multinuclear (BBO) Prodigy CryoProbe. Infrared spectra were recorded on a Shimadzu IR-Affinity 1S FTIR spectrometer in ATR mode with a diamond mono-crystal. High resolution ESI mass spectra were performed on a Waters LCT HR time of flight mass spectrometer in positive ion mode or in a Waters GCT Premier micromass time of flight spectrometer. High resolution APCI mass spectra were performed on a Waters LCT Premier quadrupole time of flight mass spectrometer operating in atmospheric pressure chemical ionization mode.

Computational details: Calculations and geometry optimizations were carried out using S3 Gaussian 09 including the D01 revision at the B3LYP/cc-pVTZ level of theory. The AICD surfaces have been calculated using AICD software, developed by Herges and Geuenich.

Synthesis of 2^H: To a solution of 2,2'-dibromonaphthalene (4.0 g, 9.7 mmol) in dry THF (130 mL) TMEDA (3.2 mL, 22 mmol) was added under N_2. *n*-BuLi (1.6 M solution in hexanes) (14.7 mL, 23.3 mmol) was added dropwise at -96 °C and the reaction mixture

stirred for 1 h. To the green slurry which formed $(MeS)_2$ (4.4 mL, 49 mmol) was added at -96 °C, and the yellow mixture was stirred overnight while allowed to slowly return back to rt. Water (50 mL) was added and the mixture extracted with CH_2Cl_2 (3 × 50 mL). The organic phase was dried with $MgSO_4$, filtered and concentrated in vacuo with a liquid N_2 trap. The crude was purified through silica gel chromatography (petroleum ether/CH_2Cl_2, 4:1) to give **2^H** as a white solid (2.76 g, 82%).

M.p.: 182-183 °C; IR (ATR) v (cm^{-1}): 3051, 2980, 2914, 1616, 1580, 1557, 1499, 1421, 1335, 1310, 1258, 1211, 1200, 1159, 1132, 1117, 1057, 1024, 951, 943, 856, 800, 777, 772, 745, 737, 691, 669, 610, 559; ^{1}H NMR (400 MHz, CD_2Cl_2): δ = 8,01 (d, J = 8.8 Hz, 2H), 7.92 (d, J = 8.2 Hz, 2H), 7.62 (d, J = 8.8 Hz, 2H), 7.41 (ddd, J = 8.2, 6.8, 1.3 Hz, 2H), 7.25 (ddd, J = 8.5, 6.8, 1.3 Hz, 2H), 6.96 (d, J = 8.5 Hz, 2H), 2.44 (s, 6H); ^{13}C NMR (100 MHz, $CDCl_3$): δ = 136.7, 132.7, 132.6, 131.5, 129.0, 128.3, 127.1, 125.3, 125.0, 132.3, 15.9; HRMS (ES^+): m/z $[M+H]^+$ calcd for ($C_{22}H_{19}S_2$): 347.0928; found 347.0928.

Synthesis of 2^{Br}: To a solution of compound 2^H (1.00 g, 2.89 mmol) in dry CH_2Cl_2 (10 mL) a bromine solution was added dropwise (0.4 mL, 7.8 mmol of bromine in 9.6 mL of dry CH_2Cl_2) at 0 °C, under N_2. The mixture was stirred overnight while allowed to slowly reach rt. The reaction mixture was quenched by the addition of saturated $Na_2S_2O_3$ solution (20 mL) and extracted with CH_2Cl_2 (3 x 50 mL). The combined organic phases were washed with brine, dried over $MgSO_4$, filtered and concentrated in vacuo. The crude was purified by silica gel chromatography (petroleum ether/CH_2Cl_2 5:1) to afford 2^{Br} as a white solid (1.31 g, 90%).

M.p.: 247-250 °C (decomposition); IR (ATR) v (cm^{-1}): 3067, 3048, 2957, 2916, 2853, 1730, 1724, 1719, 1576, 1558, 1545, 1485, 1429, 1331, 1308, 1287, 1273, 1263, 1254, 1153, 1142, 1123, 1072, 1065, 972, 947, 870, 818, 808, 795, 760, 737, 702, 671, 646, 517; ^{1}H NMR (300 MHz, CD_2Cl_2): δ = 8.08 (d, J = 2.1 Hz, 2H), 7.92 (d, J

= 8.8 Hz, 2H), 7.63 (d, *J* = 8.8 Hz, 2H), 7.32 (dd, *J* = 9.0, 2.1 Hz, 2H), 6.81 (d, *J* = 9.0, 2H), 2.43 (s, 6H); ^{13}C NMR (100 MHz, $CDCl_3$): δ = 137.6, 132.5, 131.7, 131.0, 130.6, 130.4, 128.3, 126.5, 124.2, 119.4, 15.7; HRMS (EI$^+$): m/z $[M]^+$ calcd for ($C_{22}H_{16}{}^{79}Br^{81}BrS_2$): 503.9040; found 503.9036.

Synthesis of 2^{Oct}: To a suspension of **2^{Br}** (390 mg, 0.773 mmol) and [Pd(dppf)Cl_2] (29 mg, 0.039 mmol) in dry THF (25 mL) under N_2, *n*-Oct-Mg-Br was added dropwise (3.8 mL of 1 M solution in THF) at 0 °C. The mixture was stirred at reflux for 2.5 h and then at rt overnight. NH_4Cl aq. sat. solution (20 mL) was added, and the mixture extracted with EtOAc (3 x 20 mL). The combined organic phases were washed with brine, dried over $MgSO_4$, filtered and concentrated in vacuo. The crude product was purified by silica gel chromatography (petroleum ether/CH_2Cl_2 5:1), to afford **2^{Oct}** (310 mg, 70%) as a white glue.

IR (ATR) v (cm^{-1}): 2955, 2920, 2853, 1578, 1493, 1458, 1433, 1377, 1335, 1312, 1260, 1140, 1119, 974, 880, 843, 802, 721, 679, 420; ^{1}H NMR (300 MHz, $CDCl_3$): δ = 7.91 (d, *J* = 8.7 Hz, 2H), 7.65 (d, *J* = 1.7 Hz, 2H), 7.55 (d, *J* = 8.7 Hz, 2H), 7.09 (dd, *J* = 8.7, 1.7 Hz, 2H), 6.92 (d, *J* = 8.7 Hz, 2H), 2.72-2.62 (m, 4 H), 2.42 (s, 6H), 1.68 – 1.63 (m, 4H), 1.40 – 1.26 (m, 20H), 0.89 – 0.85 (m, 6H); ^{13}C NMR (75 MHz, $CDCl_3$): δ = 139.9, 135.3, 132.7, 131.7, 131.2, 128.7, 128.5, 126.6, 124.9, 123.4, 36.1, 32.0, 31.3, 29.6, 29.6, 29.4, 22.8, 16.0, 14.3; HRMS (APCI$^+$): m/z $[M+H]^+$ calcd for ($C_{38}H_{51}S_2$): 571.3432; found 571.3435.

Synthesis of 4^{H} and 4^{Oct}: To an oven dried flask containing compound **3^{H}** (100 mg, 0.264 mmol) or **3^{Oct}** (500 mg, 0.829 mmol) in 65 mL of dry CH_3CN, TfOH (1 mL) was added under N_2, and the mixture stirred at 80 °C overnight. Pyridine (5 mL) was added to the reaction mixture and stirred overnight at 80 °C. After cooling to rt, pyridine was removed in vacuo, the residue dissolved in CH_2Cl_2, washed with water and brine, dried with $MgSO_4$, filtered and concentrated. The crude product was purified

by column chromatography (neutral alumina Brockman activity 1, hexane/CH_2Cl_2 20:1, gradient to pure CH_2Cl_2) to afford **4^H** as an orange solid (37 mg, 45%) and **4^{Oct}** as an orange solid (140 mg, 31%).

4^H: M.p.: 211-213 °C; IR (ATR) ν (cm^{-1}): 3042, 2920, 2851, 1593, 1543, 1508, 1499, 1474, 1458, 1414, 1358, 1315, 1281, 1206, 1163, 1155, 1115, 1074, 995, 966, 959, 874, 812, 777, 758, 744, 640, 630, 557, 550, 530; ^1H NMR (300 MHz, CD_2Cl_2): δ = 7.27 (d, J = 8.7 Hz, 2H), 7.13 (dd, J = 8.1 Hz, 1.4 Hz, 2H), 7.01 (dd, J = 8.1, 7.3 Hz, 2H), 6.86 (dd, J = 7.3 Hz, 1.4 Hz, 2H), 6.79 (d, J = 8.7 Hz, 2H); ^{13}C NMR (75 MHz, $CDCl_3$): δ = 134.3 (C), 129.9 (C), 129.7 (C), 128.7 (CH), 126.2 (CH), 125.9 (C), 125.7 (C), 125.5 (CH), 125.2 (CH), 120.9 (CH); HRMS (APCI$^+$): m/z $[M+H]^+$ calcd for ($C_{20}H_{11}S_2$): 315.0302; found 315.0293.

4^{Oct}: M.p.: 120-122 °C; IR (ATR) ν (cm^{-1}): 3051, 2949, 2922, 2853, 1609, 1547, 1487, 1466, 1420, 1360, 1283, 1169, 1111, 1009, 941, 870, 839, 795, 773, 735, 554; ^1H NMR (300 MHz, $CDCl_3$): δ = 7.18 (d, J = 8.7 Hz, 2H), 6.88 (d, J = 1.6 Hz, 2H), 6.74 (d, J = 8.7 Hz, 2H), 6.72 (d, J = 1.6 Hz, 2H), 2.50 – 2.45 (m, 4H), 1.58 (m, 4H), 1.31 – 1.26 (m, 20H), 0.88 – 0.86 (m, 6H); ^{13}C NMR (75 MHz, $CDCl_3$): δ = 141, 134.6, 129.6, 128.4, 128.3, 125.6, 125.6, 124.9, 124.1, 122.0, 35.5, 32.0, 30.9, 29.6, 29.4, 29.4, 22.8, 14.3; HRMS (EI$^+$): m/z $[M]^+$ calcd for ($C_{36}H_{42}S_2$): 538.2728; found 538.2715.

Synthesis of 7^H: To a suspension of **4^H** (25 mg, 0.066 mmol) in CH_3COOH (5 mL), H_2O_2 (1 mL) was added, and the mixture refluxed overnight. After cooling down to rt a yellow precipitate which formed was washed with water and petroleum ether, and recrystallised from hot DMF. Recrystallisation did not allow purification, as an impurity also crystallised, and low solubility of the product did not allow purification with other methods. However, despite the crystallisation of impurity, it

was possible to manually pick crystals of **7^{H}** suitable for X-Ray diffraction.

Synthesis of 7^{Oct}: To a suspension of **4^{Oct}** (30 mg, 0.056 mmol) in $CHCl_3$ (5 mL), *m*CPBA (43 mg, 0.25 mmol) was added, and the mixture refluxed overnight. The mixture was cooled down to rt and concentrated under reduced pressure. The crude product was purified with silica gel chromatography (petroleum ether/CH_2Cl_2 1:4, gradient to 2:5) to afford **7^{Oct}** (27 mg, 90%) as a pale, yellowish solid.

M.p.: 184-186 °C; IR (ATR) ν (cm^{-1}): 2957, 2922, 2847, 1618, 1582, 1466, 1433, 1422, 1371, 1290, 1206, 1159, 1134, 1123, 1013, 974, 895, 822, 799, 775, 719, 662, 611, 588, 569, 557, 519; ^{1}H NMR (300 MHz, CD_2Cl_2): δ = 8.50 (d, J = 1.7 Hz, 2H), 8.45 (d, J = 8.7 Hz, 2H), 8.27 (d, J = 8.7 Hz, 2H), 8.11 (d, J = 1.7 Hz , 2H), 3.00 – 2.95 (m, 4H), 1.87 – 1.77 (m, 4H), 1.45- 1.29 (m, 20H), 0.90 – 0.86 (m, 6H); ^{13}C NMR (75 MHz, CD_2Cl_2): δ = 145.0, 136.0, 135.3, 134.2, 134.0, 132.5, 128.7, 123.0, 121.9, 121.6, 36.2, 32.4, 31.3, 29.9, 29.8, 29.8, 23.2, 14.4; HRMS (APCI^{+}): m/z $[M+H]^{+}$ calcd for ($C_{36}H_{43}O_4S_2$): 603.2603; found 603.2603.

Synthesis of 8: To a stirred solution of 2,2′-dibromo-1,1′-binaphthalene (500 mg, 1.21 mmol) in dry THF (20 mL), TMEDA (0.40 mL, 2.7 mmol) was added under N_2. *n*-BuLi (1.6 M solution in hexanes) (1.8 mL, 2.9 mmol) was added dropwise at -78 °C and the mixture stirred for 1h. To the formed, greenish slurry $(MeSe)_2$ (0.69 mL, 7.3 mmol) was added dropwise at -78 °C, and the reaction mixture was stirred overnight while slowly heating back to rt. Water (20 mL) was added and the mixture extracted with CH_2Cl_2 (3 x 20 mL). The combined organic phases were dried with $MgSO_4$, filtered and concentrated in vacuo. Purification by silica gel chromatography with petroleum ether/CH_2Cl_2 (4:1) gave desired product **8** as a white solid (345 mg, 65% yield).

M.p.: 174 - 176 °C; IR (ATR) ν (cm^{-1}): 3049, 2980, 2928, 1614, 1578, 1555, 1499, 1420, 1395, 1373, 1339, 1317, 1273, 1254, 1165,

1150, 1134, 1125, 1107, 941, 910, 901, 843, 804, 779, 770, 743, 689, 546; ^{1}H NMR (300 MHz, $CDCl_3$): δ = 7.94 (d, *J* = 8.7 Hz, 2H), 7.90 (d, *J* = 8.2 Hz, 2H), 7.64 (d, *J* = 8.7 Hz, 2H), 7.43 (ddd, *J* = 8.2, 6.8, 1.3 Hz, 2H), 7.25 (ddd, *J* = 8.5, 6.8, 1.3 Hz, 2H), 7.04 (d, *J* = 8.5 Hz, 2H), 2.28 (s, 6H); ^{13}C NMR (75 MHz, $CDCl_3$) δ = 135.6, 132.7, 132.3, 132.0, 129.0, 128.3, 127.1, 125.8, 125.5, 125.1, 6.6; HRMS (APCI$^+$): m/z $[M+H]^+$ calcd for ($C_{22}H_{19}{}^{78}Se_2$): 438.9833; found: 438.9840.

Synthesis of 10: To a two-neck oven-dried flask fitted with a condenser, compound **9** (50 mg, 0.11 mmol) was added under N_2. TfOH (0.3 mL) was added, and the mixture stirred at 80 °C overnight. Pyridine (1.5 mL) was added, and the mixture stirred overnight at 100 °C. The cooled mixture was diluted with toluene, transferred to a round bottom flask and evaporated under reduced pressure. Water was added and the mixture extracted with toluene (1 x 50 mL). The organic phase was washed with water (3 x 20 mL) and brine (1 x 20 mL), dried with $MgSO_4$ and concentrated in vacuo. Recrystallisation from hot toluene and hexane mixture afforded **10** as red needles (19 mg, 44%).

M.p.: 166 - 168 °C; IR (ATR) ν (cm^{-1}): 3046, 2980, 2889, 1717, 1595, 1541, 1506, 1456, 1418, 1395, 1387, 1339, 1258, 1204, 1157, 1105, 1070, 957, 806, 772, 746, 627, 546; ^{1}H NMR (300 MHz, $CDCl_3$): δ = 7.46 (d, *J* = 8.5 Hz, 2H), 7.36 (dd, *J* = 7.9, 1.4 Hz, 2H), 7.28 (dd, *J* = 7.3 Hz, 1.4 Hz, 2H), 7.19 (d, *J* = 8.5 Hz, 2H), 7.14 (dd, *J* = 7.9 Hz, 7.3 Hz, 2H); ^{13}CNMR could not me recorded due to poor solubility. HRMS (APCI$^+$): m/z $[M+H]^+$ calcd for ($C_{20}H_{11}{}^{78}Se^{80}Se$): 408.9199; found: 408.9187.

General procedure for chemical oxidation: To a solution of the relevant PTXTX derivative in 20 – 80 mL of 1:1 $CHCl_3$:CH_3COOH mixture, H_2O_2 (30 – 35% in water) was added and the mixture stirred for 4 – 6 h at rt. The reaction mixture was quenched with saturated NaOH aq. solution at 0 °C, until pH~12. The mixture was extracted with $CHCl_3$. The combined organic phases

were washed with brine, dried over $MgSO_4$, filtered and concentrated in vacuo.

3^{H}: M.p.: 142-145 °C; IR (ATR) ν (cm^{-1}): 3055, 2997, 2913, 1584, 1503, 1412, 1403, 1308, 1256, 1161, 1032, 951, 872, 818, 787, 775, 748, 692, 677, 637, 496, 463; ^{1}H NMR (300 MHz, CD_2Cl_2) and ^{13}C NMR (75 MHz, $CDCl_3$) spectra of the diastereoisomeric mixture available in the SI; HRMS (ES^+): m/z $[M+H]^+$ calcd for ($C_{22}H_{19}O_2S_2$): 379.0826; found 379.0829.

3^{Oct}: IR (ATR) ν (cm^{-1}): 2853, 2361, 2342, 1578, 1491, 1458, 1433, 1375, 1337, 1312, 1258, 1119, 1057, 880, 814, 802, 669, 419; ^{1}H NMR (300 MHz, $CDCl_3$) and ^{13}C NMR (75 MHz, $CDCl_3$) spectra of the diastereoisomeric mixture available in the SI. HRMS ($APCI^+$): m/z $[M+H]^+$ calcd for ($C_{38}H_{51}O_2S_2$): 603.3330; found 603.3340.

5^{H}: M.p.: 240-242 °C; IR (ATR) ν (cm^{-1}): 3048, 2918, 2851, 1609, 1541, 1495, 1435, 1416, 1341, 1290, 1229, 1196, 1140, 1059, 1016, 959, 874, 854, 829, 816, 783, 752, 685, 673, 646, 604, 567, 530, 515, 496, 465, 453, 434, 409; ^{1}H NMR (300 MHz, $CDCl_3$): δ = 8.38 (dd, J = 7.2, 1.3 Hz, 1H), 8.14 (dd, J = 8.0, 1.3 Hz, 1H), 7.95 (d, J = 8.5 Hz, 1H), 7.93 (d, J = 8.7 Hz, 1H), 7.81 (dd, J = 8.0, 7.2 Hz, 1H), 7.80 (d, J = 8.7 Hz,1H), 7.59 (dd, J = 7.6, 1.8 Hz, 1H), 7.48 – 7.43 (m, 2H), 7.41 (dd, J = 7.4, 1.8 Hz, 1H); ^{13}C NMR spectra could not be recorded due to low solubility of the product; HRMS ($APCI^+$): m/z $[M+H]^+$ calcd for ($C_{20}H_{11}OS_2$): 331.0251; found 331.0255.

5^{Oct}: M.p.: 142-144 °C; IR (ATR) ν (cm^{-1}): 3049, 2951, 2914, 2847, 1611, 1558, 1514, 1489, 1458, 1150, 1072, 1022, 982, 939, 880; ^{1}H NMR (500 MHz, CD_2Cl_2): δ = 8.21 (d, J = 1.7 Hz, 1H), 7.95 (d, J = 1.2 Hz, 1H), 7.92 (d, J = 8.7 Hz, 1H), 7.90 (d, J = 8.6 Hz, 1H), 7.76 (d, J = 8.6 Hz, 1H), 7.47 (d, J = 8.7 Hz, 1H), 7.41 (d, J = 1.2 Hz, 1H), 7.32 (d, J = 1.7 Hz, 1H), 2.95 – 2.91 (m, 2H), 2.75 – 2.72 (m, 2H), 1.80 – 1.77 (m, 2H), 1.72 – 1.70 (m, 2H), 1.41 – 1.27 (m, 20H), 0.89 – 0.87 (m, 6H); ^{13}C NMR (75 MHz, $CDCl_3$): δ = 142.8 (C), 141.6 (C), 137.6 (C), 134.9 (CH), 134.8

(C), 132.7 (CH), 132.6 (C), 131.7 (C), 131.1 (C), 130.8 (CH), 129.6 (CH), 128.8 (CH), 128.0 (C), 127.2, (C), 126.5 (C), 126.0 (CH), 124.1 (CH), 122.1 (CH), 121.4 (C), 119.6 (C), 35.8 (CH_2), 35.6 (CH_2), 32.0 (CH_2), 31.2 (CH_2), 31.1 (CH_2), 29.6 (CH_2), 29.5 (CH_2), 29.4 (CH_2), 22.8 (CH_2), 14.3 (CH_3) (6 carbon peaks are missing due to overlap); HRMS (APCI$^+$): m/z $[M+H]^+$ ($C_{36}H_{43}OS_2$): 555.2755; found 555.2758.

6^H: m.p.: 284-286 °C (decomposition); IR (ATR) ν (cm^{-1}): 3090, 3055, 3011, 2924, 2853, 1578, 1489, 1423, 1369, 1294, 1215, 1202, 1153, 1142, 1121, 1061, 1013, 835; ^{1}H NMR (300 MHz, CD_2Cl_2): δ = 8.43 (dd, J = 7.2, 1.2 Hz, 2H), 8.38 (dd, J = 7.2, 1.2 Hz, 2H), 8.30 – 8.27 (m, 8H), 8.23 (dd, J = 8.2, 1.2 Hz, 2H), 8.16 (dd, J = 8.2, 1.2 Hz, 2H), 7.92 – 7.84 (m, 4H); ^{13}C NMR (75 MHz, $CDCl_3$): δ = 137.7 (C), 136.8 (C), 136.5 (C), 135.8 (C), 135.2 (C), 134.6 (C), 133.4 (CH), 132.6 (CH), 132.3 (CH), 132.3 (CH), 131.5 (CH), 129.2 (CH), 128.1 (CH), 128.1 (CH), 126.5 (CH), 124.5 (CH), 122.4 (C), 122.1 (C) (2 carbon peaks are missing due to overlap); HRMS (APCI$^+$): m/z $[M+H]^+$ ($C_{20}H_{11}O_2S_2$): 347.0200; found 347.0211.

9: IR (ATR) ν (cm-1): 3055, 2982, 1501, 1396, 1308, 1258, 1157, 1072, 899, 876, 799, 775, 748, 687, 671, 625; ^{1}H NMR (300 MHz, CDCl3) spectra of the diastereoisomeric mixture available in the SI. ^{13}C spectra not recorded due to low solubility. HRMS (APCI+): m/z [M+H]+ calcd for (C22H19O278Se2): 470.9731; found: 470.9745.

Crystallographic details: Deposition Numbers <url href="https://www.ccdc.cam.ac.uk/services/structures?id=doi:10.1002/chem.202203115"> 1869244 and 1869246 (for **4^H**), 1869239 (for **4^{Oct}**), 1869245 (for **5^H**), 1869242 (for **5^{Oct}**), 1869243 (for **t-6^H**), 1869240 (for **7^H**), 1914850 (for **anti-7^{Oct}**), 1914851 (for **syn-7^{Oct}**), 2194810 (for **10**), 1869241 (for **11^H**), 2011130 (for (**4^H**)$_3$(ClO_4)$_2$), 2011129 (for (**PXX**)$_2$(ClO_4)$_1$)</url> contain the supplementary crystallographic data for this paper. These data are provided free of charge by the joint Cambridge Crystallographic Data

Centre and Fachinformationszentrum Karlsruhe <url href=" http://www.ccdc.cam.ac.uk/structures">Access Structures service</url>.

Acknowledgements

D.B. gratefully acknowledges the EU through the MSCA-ITN-ETN (project: PHOTOTRAIN, No. 722591) and MSCA-RISE (project: INFUSION, No. 734834) programs and the University of Vienna for generous financial support. O.M. and T.B. thank the ITN-ETN PHOTOTRAIN project for their PhD fellowships. R.D.C. acknowledges the European Union's Horizon 2020 research and innovation FET-OPEN under the grant agreement ARTIBLED No 863170, the ERC-Co InOutBioLight No. 816856, and the MSCA-ITN StiBNite No. 956923.

Keywords: mixed-valence complexes, organic semiconductors, polycyclic aromatic hydrocarbons, PXX, S-doping, thin-film lighting.

References

[1] A. Borissov, Y. K. Maurya, L. Moshniaha, W.-S. Wong, M. Żyła-Karwowska, M. Stępień, *Chem. Rev.* **2022**, *122*, 565–788.

[2] A. Narita, X. Y. Wang, X. Feng, K. Müllen, *Chem. Soc. Rev.* **2015**, *44*, 6616–6643.

[3] M. Stępień, E. Gońka, M. Żyła, N. Sprutta, *Chem. Rev.* **2017**, *117*, 3479–3716.

[4] P. G. Campbell, A. J. V Marwitz, S.-Y. Liu, *Angew. Chem. Int. Ed.* **2012**, *51*, 6074–6092.

[5] D. L. Crossley, R. J. Kahan, S. Endres, A. J. Warner, R. A. Smith, J. Cid, J. J. Dunsford, J. E. Jones, I. Vitorica-Yrezabal, M. J. Ingleson, *Chem. Sci.* **2017**, *8*, 7969–7977.

[6] Z. X. Giustra, S.-Y. Liu, *J. Am. Chem. Soc.* **2018**, *140*, 1184–1194.

[7] J. M. Farrell, C. Mützel, D. Bialas, M. Rudolf, K. Menekse, A. M. Krause, M. Stolte, F. Würthner, *J. Am. Chem. Soc.* **2019**, *141*, 9096–9104.

[8] J. P. Mora-Fuentes, A. Riaño, D. Cortizo-Lacalle, A. Saeki, M. Melle-Franco, A. Mateo-Alonso, *Angew. Chem. Int. Ed.* **2019**, *58*, 552–556.

[9] I. Michalsky, V. Gensch, C. Walla, M. Hoffmann, F. Rominger, T. Oeser, P. Tegeder, A. Dreuw, M. Kivala, *Chem. Eur. J.* **2022**, *22*, e202200326.

[10] A. Riaño, K. Strutyński, M. Liu, C. T. Stoppiello, B. Lerma-Berlanga, A. Saeki, C. Martí-Gastaldo, A. N. Khlobystov, G. Valenti, F. Paolucci, M. Melle-Franco, A. Mateo-Alonso, *Angew. Chem. Int. Ed.* **2022**, *61*, e202113657.

[11] Z. Wang, T. Baumgartner, *Chem. Rec.* **2015**, *15*, 199–217.

[12] M. Stolar, J. Borau-Garcia, M. Toonen, T. Baumgartner, *J. Am. Chem. Soc.* **2015**, *137*, 3366–3371.

[13] C. Romero-Nieto, A. de Cózar, E. Regulska, J. B. Mullenix, F. Rominger, P. Hindenberg, *Chem. Commun.* **2021**, *57*, 7366–7369.

[14] P. Hindenberg, F. Rominger, C. Romero-Nieto, *Angew. Chem. Int. Ed.* **2021**, *60*, 766–773.

[15] B. T. Luppi, A. V. Muralidharan, N. Ostermann, I. T. Cheong, M. J. Ferguson, I. Siewert, E. Rivard, *Angew. Chem. Int. Ed.* **2022**, *61*, e202114586.

[16] K. Takaishi, S. Hinoide, T. Matsumoto, T. Ema, *J. Am. Chem. Soc.* **2019**, *141*, 11852–11857.

[17] S.-F. Zhang, X.-K. Chen, J.-X. Fan, A.-M. Ren, *Org. Electron.* **2013**, *14*, 607–620.

[18] C. H. E. Chow, H. Phan, X. Zhang, J. Wu, *J. Org. Chem.* **2020**, *85*, 234–240.

[19] M. Feofanov, V. Akhmetov, R. Takayama, K. Y. Amsharov, *J. Org. Chem.* **2021**, *86*, 14759–14766.

[20] H. Ebata, E. Miyazaki, T. Yamamoto, K. Takimiya, *Org. Lett.* **2007**, *9*, 4499–4502.

[21] A. Patra, Y. H. Wijsboom, L. J. W. Shimon, M. Bendikov, *Angew. Chem. Int. Ed.* **2007**, *46*, 8814–8818.

[22] A. Patra, Y. H. Wijsboom, S. S. Zade, M. Li, Y. Sheynin, G. Leitus, M. Bendikov, *J. Am. Chem. Soc.* **2008**, *130*, 6734-6736.

[23] G. He, W. Torres Delgado, D. J. Schatz, C. Merten, A. Mohammadpour, L. Mayr, M. J. Ferguson, R. McDonald, A. Brown, K. Shankar, E. Rivard, *Angew. Chem. Int. Ed.* **2014**, *53*, 4587–4591.

[24] S. M. Parke, M. P. Boone, E. Rivard, *Chem. Commun.* **2016**, *52*, 9485–9505.

[25] A. Rossignon, D. Bonifazi, *Synthesis* **2019**, *51*, 3588–3599.

[26] T. Miletić, A. Fermi, I. Orfanos, A. Avramopoulos, F. De Leo, N. Demitri, G. Bergamini, P. Ceroni, M. G. Papadopoulos, S. Couris, D. Bonifazi, *Chem. Eur. J.* **2017**, *23*, 2363–2378.

[27] L. Dordević, D. Milano, N. Demitri, D. Bonifazi, *Org. Lett.* **2020**, *22*, 4283–4288.

[28] R. Pummerer, E. Prell, A. Rieche, *Ber. Dtsch. Chem. Ges.* **1926**, *59*, 2159–2161.

[29] N. Kobayashi, M. Sasaki, K. Nomoto, *Chem. Mater.* **2009**, *21*, 552–556.

[30] T. Kamei, M. Uryu, T. Shimada, *Org. Lett.* **2017**, *19*, 2714–2717.

[31] N. Kobayashi, M. Sasaki, T. Ohe, *Semiconductor Device, Method of Manufacturing the Same, and Method of Forming Multilayer Semiconductor Thin Film*, **2013**, US20130200343A1.

[32] D. Stassen, N. Demitri, D. Bonifazi, *Angew. Chem. Int. Ed.* **2016**, *55*, 5947–5951.

[33] A. Berezin, N. Biot, T. Battisti, D. Bonifazi, *Angew. Chem. Int. Ed.* **2018**, *57*, 8942–8946.

[34] A. Sciutto, A. Fermi, A. Folli, T. Battisti, J. M. Beames, D. M. Murphy, D. Bonifazi, *Chem. Eur. J.* **2018**, *24*, 4382–4389.

[35] A. Sciutto, A. Berezin, M. Lo Cicero, T. Miletić, A. Stopin, D. Bonifazi, *J. Org. Chem.* **2018**, *83*, 13787–13798.

[36] N. Lv, M. Xie, W. Gu, H. Ruan, S. Qiu, C. Zhou, Z. Cui, *Org. Lett.* **2013**, *15*, 2382–2385.

[37] N. Xu, Y. Li, R. Wu, R. Zhu, J. Zhang, S. M. Zakeeruddin, H. Li, Z. S. Li, M. Grätzel, P. Wang, *Chem. Eur. J.* **2019**, *25*, 945–948.

[38] L. Đorđević, C. Valentini, N. Demitri, C. Mézière, M. Allain, M. Sallé, A. Folli, D. Murphy, S. Mañas-Valero, E. Coronado, D. Bonifazi, *Angew. Chem. Int. Ed.* **2020**, *59*, 4106–4114.

[39] J. Fletcher-Charles, R. R. Ferreira, M. Abraham, D. Romito, M. Oppel, L. González, D. Bonifazi, *Eur. J. Org. Chem.* **2022**, *2022*, e202101166.

[40] J. Yuan, Z. Xu, M. O. Wolf, *Chem. Sci.* **2022**, *13*, 5447–5464.

[41] A. Wigglesworth, Y. Wu, P. Liu, *Thiaxanthenothiaxanthene Semiconductor Compound for TFTs*, **2012**, DE102012201975A1.

[42] A. Zheng, M. Ren, Y. Zhang, Y. Cai, J. Zhang, Y. Yuan, M. Lei, P. Wang, *ACS Mater. Lett.* **2020**, *2*, 691–698.

[43] Y. Zhou, W.-J. Liu, Y. Ma, H. Wang, L. Qi, Y. Cao, J. Wang, J. Pei, *J. Am. Chem. Soc.* **2007**, *129*, 12386–12387.

[44] J. A. Fernández-Salas, A. P. Pulis, D. J. Procter, *Chem. Commun.* **2016**, *52*, 12364–12367.

[45] C. Du, S. Ye, Y. Liu, Y. Guo, T. Wu, H. Liu, J. Zheng, C. Cheng, M. Zhu, G. Yu, *Chem. Commun.* **2010**, *46*, 8573–8575.

[46] R. Al-Aqar, A. C. Benniston, A. Harriman, T. Perks, *ChemPhotoChem* **2017**, *1*, 198–205.

[47] A. Kremer, C. Aurisicchio, F. Deleo, B. Ventura, J. Wouters, N. Armaroli, A. Barbieri, D. Bonifazi, *Chem. Eur. J.* **2015**, *21*, 15377–15387.

[48] M. Kasha, *J. Chem. Phys.* **1952**, *20*, 71–74.

[49] C. Würth, M. Grabolle, J. Pauli, M. Spieles, U. Resch-Genger, *Nat. Protoc.* **2013**, *8*, 1535–1550.

[50] K. Suzuki, A. Kobayashi, S. Kaneko, K. Takehira, T. Yoshihara, H. Ishida, Y. Shiina, S. Oishi, S. Tobita, *Phys. Chem. Chem. Phys.* **2009**, *11*, 9850–9860.

[51] G. Givaja, P. Amo-Ochoa, C. J. Gómez-García, F. Zamora, *Chem. Soc. Rev.* **2012**, *41*, 115–147.

[52] R. D. Costa, *Light-Emitting Electrochemical Cells. Concepts, Advances and Challenges*, Springer International Publishing: Basel, **2017**.

[53] E. Fresta, R. D. Costa, *J. Mater. Chem. C* **2017**, *5*, 5643–5675.

[54] S. Tang, L. Edman, *Top. Curr. Chem.* **2016**, *374*, 40.

[55] E. Fresta, K. Baumgärtner, J. Cabanillas-Gonzalez, M. Mastalerz, R. D. Costa, *Nanoscale Horiz* **2020**, *5*, 473–480.

[56] E. Fresta, J. Dosso, J. Cabanillas-Gonzalez, D. Bonifazi, R. D. Costa, *ACS Appl. Mater. Interfaces* **2020**, *12*, 28426–28434.

[57] E. Fresta, J. Dosso, J. Cabanillas-González, D. Bonifazi, R. D. Costa, *Adv. Funct. Mater.* **2020**, *30*, 1906830.

[58] M. D. Weber, M. Adam, R. R. Tykwinski, R. D. Costa, *Adv. Funct. Mater.* **2015**, *25*, 5066–5074.

[59] K. Shanmugasundaram, M. S. Subeesh, C. D. Sunesh, R. K. Chitumalla, J. Jang, Y. Choe, *J. Phys. Chem. C* **2016**, *120*, 20247–20253.

[60] M. S. Subeesh, K. Shanmugasundaram, C. D. Sunesh, Y. S. Won, Y. Choe, *J. Mater. Chem. C* **2015**, *3*, 4683–4687.

[61] M. S. Subeesh, K. Shanmugasundaram, C. D. Sunesh, R. K. Chitumalla, J. Jang, Y. Choe, *J. Phys. Chem. C* **2016**, *120*, 12207–12217.

[62] M. S. Subeesh, K. Shanmugasundaram, C. D. Sunesh, T. P. Nguyen, Y. Choe, *J. Phys. Chem. C* **2015**, *119*, 23676–23684.

[63] K. Shanmugasundaram, R. K. Chitumalla, J. Jang, Y. Choe, *New J. Chem.* **2017**, *41*, 9668–9673.

[64] S. Kanagaraj, A. Puthanveedu, Y. Choe, *Adv. Funct. Mater.* **2020**, *30*, 1907126.

[65] K. Shanmugasundaram, J. C. John, S. Chitumalla, J. Jang, Y.

Choe, *Org. Electron.* **2019**, *67*, 141–145.

[66] K. Shanmugasundaram, H. Been, J. C. John, A. Puthanveedu, N. N. T. Pharm, S. G. Lee, Y. Choe, *New J. Chem.* **2021**, *45*, 19338–19346.

[67] K. Jongseong, K. Shanmugasundaram, R. K. Chitumalla, J. Jang, Y. Choe, *J. Lumin.* **2018**, *197*, 383–388.

[68] S. Tang, A. Sandström, P. Lundberg, T. Lanz, C. Larsen, S. Van Reenen, M. Kemerink, L. Edman, *Nat. Commun.* **2017**, *8*, 1–9.

[69] J. C. John, K. Shanmugasundaram, C. V. S. Brahmmananda Rao, G. Gopakumar, Y. Choe, *J. Phys. Chem. C* **2021**, *125*, 17993–18001.

[70] J. C. John, K. Shanmugasundaram, C. V. S. Brahmmananda Rao, G. Gopakumar, Y. Choe, *New J. Chem.* **2021**, *45*, 12576–12584.

10.1002/chem.202203115

Entry for the Table of Contents

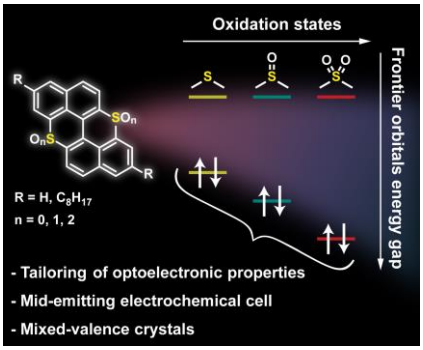

Peri-thiaxanthenothiaxanthene is used as functional scaffold to engineer molecular semiconductor the properties of which can be tailored by editing the oxidation state of the S-atoms. Oxidation with H_2O_2 led to the relevant sulfoxide and sulfone congeners, whereas electrooxidation yields to sulfonium-type derivatives forming crystalline mixed valence complexes. The semiconducting properties were tested in light-emitting electrochemical cells (LECs), obtaining the first mid-emitting S-doped PAH-based LECs.

Researcher Twitter usernames: @BonifaziGroup
Website: https://bonifazi-group.univie.ac.at